FoxO3a is an anti-aging factor for age-related skin atrophy and pigmentation

（FoxO3aは皮膚老化による萎縮や色素沈着を抑制する因子である）

千葉大学大学院医学薬学府

先端医学薬学専攻

（主任：横手幸太郎教授）

金　周元

Abstract

Aging is characterized by accumulation of chronic and irreversible oxidative damage, chronic inflammation, and organ dysfunction. Superoxide dismutase (SOD) serves as a major enzyme for cellular superoxide radical metabolism and physiologically regulates cellular redox balance throughout the body. The copper/zinc superoxide dismutase (SOD1)-deficient mice showed diverse phenotypes associated with enhanced oxidative damage in whole organs.

Here, I found that oral treatment with syringaresinol (SYR, also known as lirioresinol B), which is the active component in the berries of Korean ginseng (*Panax ginseng* C.A.Meyer), attenuated the age-related changes in *Sod1*$^{-/-}$ skin. Interestingly, SYR morphologically normalized skin atrophy in *Sod1*$^{-/-}$ mice and promoted fibroblast outgrowth from *Sod1*$^{-/-}$ skin *in vitro*. These protective effects were mediated by the suppression of matrix metalloproteinase-2 (MMP-2) overproduction in *Sod1*$^{-/-}$ skin, but not by increased collagen expression. SYR also decreased the oxidative damage and the phosphorylation of forkhead box O3a (FoxO3a) protein, which was a transcriptional factor of MMP-2, in *Sod1*$^{-/-}$ skin.

On the other hand, in skin cells, melanin formation is critical factor for not only melanoma but also sun burn and so on. Many of antioxidants are used to prevent excessive melanin generation because of melanogenesis involves several oxidizing process. However, melanogenesis inhibition mechanism by antioxidants is understood insufficiently.

In this report, I propose that FoxO3a is a key factor for antioxidant-mediated melanogenesis inhibition. Inhibition of FoxO3a results in the expression of melanogenic genes and melanin levels elevated. The FoxO3a overexpression by vector transfection or activation by PI3K or Akt inhibition reversed these events. When FoxO3a nuclear localization sequence harbored, anti-melanogenic effect was not observed, suggesting that FoxO3a nuclear translocation is pivotal

factor for the melanogenesis modulation. Under the condition of antioxidants treatment, melanogenesis inhibited correspond with FoxO3a activation, and FoxO3a-directed siRNA transfection abolishes these effects. These results indicate that FoxO3a acts as an essential factor for melanogenesis regulation.

Because of its response to various environmental stimuli, FoxO3a could be a remarkable target for investigating de novo anti-aging pathway and for designing pharmacological anti-aging agents.

Abbreviations: FoxO, forkhead box-O; IGF, insulin growth factor; ROS, reactive oxygen species; PI3K, phosphoinositide 3-kinase; PKB, protein kinase B; LP, light pigmented; MP, moderate pigmented; DP, darkly pigmented; SCF, stem cell factor; ckit, SCF receptor; SOX10, SRY-related HMG-box; MITF, microphthalmia-associated transcription factor; TYR, tyrosinase; TYRP1, tyrosinase-related protein 1; DCT, dopachrome delta-isomerase; PAX3, paired box transcription factor; MART1, melanoma antigen recognized by T-cells; EDNRB, endothelin receptor B; Vc, vitamin C; NAC, N-acetyl cystein

Introduction

A genetic contribution to aging can be explained by senescence-protective genes, which have been defined in long-lived populations. The forkhead/winged helix Class O transcription factors (FoxO) transcription factors have been reported as one of longevity genes. FoxO transcription factors are widely conserved in various organisms, depict a divergent cellular works that regulate expression of genes, such as the regulation of cell death, cell cycle, development, energy metabolism, DNA repair, and stress response [1-5]. Mammalian FoxO family has defined as following: FoxO1, FoxO3, FoxO4, and FoxO6. These FoxOs are triggered by diverse environmental stimulation, such as cytokines, nutrients, and insulin growth factors (IGFs). FoxOs are speculated as an essential factor for prevent aging and age-dependent diseases however, their role in skin aging has yet to be determined. The same consensus binding sequence is shared by all FoxO proteins and, can act redundantly. Also, distinct FoxO isoforms have specific functions induced by their tissue-specific manner of expression [6,7]. Each FoxO deletion mutants in mice model have uncovered specific works of FoxO isoforms [8]. In case of FoxO1 deletion mutant is lethal because of vascular development deficiency [9]. Knockout mice of FoxO3a showed early oocyte depletion by age-dependent infertility [10]. These reports demonstrate that the FoxO genes work in various cellular processes and especially, functions of FoxO3a is important in age-dependent skin events.

Each FoxO family is elaborately modulated by post-translational modifications, which affect stability, activity, and cellular localization of protein. FoxO activity is modulated by reactive oxygen species [11] either by regulating activity of growth factor receptors, serine/threonine kinases, tyrosine kinases, and phosphatases or by modulating factors that upstream of FoxO via interactions with lipid metabolism [12-14]. FoxO activity is activated or inhibited by ROS a context-

dependent manner. In case of the phosphoinositide 3-kinase (PI3K)- protein kinase B (PKB) pathway activated by hydrogen peroxide, FoxO activity was inhibited by insulin-mimetic effects [15], meanwhile ROS-activated MST1, MAPK, and JNK activate the FoxO proteins phosphorylates and abolition of binding with 14-3-3 protein [16-18]. These results represent that ROS signaling and ROS accumulation level regulates FoxO activity positively or also negatively. my previous studies have demonstrated that *Sod1*-deficient (*Sod1*$^{-/-}$) mice exhibit increased intracellular O_2^- concentrations and various aging-related organ phenotypes [19], such as age-related macular degeneration [20], fatty deposits in the liver [21,22], skin atrophy [23,24], bone loss and fragility [25,26], the progression of Alzheimer's disease [27], infertility [28], dry eyes [29,30], and rotator cuff degeneration [31]. These findings suggest that cytoplasmic O_2^--mediated oxidative damage is the primary cause of age-related changes in various tissues. Especially, knock down of Sod1 related with extracellular matrix related-genes suppression, including procollagen 1a1/*Col1a1* and hyaluronan synthase 2/*Has2*, as well as up-regulation of extracellular degrading genes such as *Mmp-1* and *Mmp-2*, results in epidermal and also dermal atrophy [24,32].

On the other hand, previous reports indicate that FoxO3a is involved in cellular processes in response to external stress in the skin cells, however FoxO3a functions in melanocytic cells has not yet been uncovered. Melanin is produced as a photo-protector against UV irradiation for the skin, which is produced by continual oxidation steps. Many antioxidants have been treated to hyperpigmentation because of their oxidative properties [33]. Additionally, the deficient phototype of skin is associated with the low activity of catalase, the main enzyme responsible for degrading hydrogen peroxide; patients with this phenotype do not tan well, burn relatively easily, and are at a higher risk of skin cancer than those with the high skin phototype [34], thereby indicating a tight association between melanogenesis and oxidative stress in the skin. However, melanogenesis

regulation by redox state has not yet been studied precise. Because activity of FoxO3a can be modulated by redox state, which in turn regulates melanin production steps, I suppose that the melanogenesis shift induced by ROS perturbation may occur by FoxO3a-mediated cell signaling.

Previously, my reports have shown that syringaresinol (4,4'-(1S,3aR,4S,6aR)-tetrahydro-1H,3H-furo[3,4-c]furan-1,4-diylbis(2,6-dimethoxyphenol, SYR), isolated from *Panax ginseng* berry pulp, activates sirtuin 1 gene expression, leading to delayed cellular senescence, and its effects were dependent on FoxO3a [35]. In the present study, I suggest that FoxO3a is a novel anti-melanogenic and anti-aging factor for skin. I investigate the feasibility that treatment with natural antioxidants can delay skin aging and pigmentation. I investigated the beneficial effects of SYR for age-dependent skin atrophy, as well as the underlying biological mechanism of melanin formation.

Results

Positive relationship of FoxO3a with melanogenesis in pigmented melanocytes

FoxO3a regulates cell cycle which results in environment-specific differentiation in various pathways [36]. Foxo3a has the reaction of keratinocytes to UV irradiation and the senescence of dermal fibroblasts in skin cells. First, I investigated the expression levels of FoxO1, FoxO3a, and FoxO4 in lightly pigmented (LP), moderately pigmented [37], and darkly pigmented (DP) melanocytes and melanoma MNT1 cells to clarify whether the FoxO genes are involved in melanocyte differentiation (Figure 1a-c). In these pigment-related cells, the expression level of FoxO3a was more than 10 fold higher levels than the other FoxO proteins (Figure 1b), and with increasing degree of pigmentation its expression levels decreased (Figure 1b-c), suggesting an adverse relationship between melanin levels and expression of FoxO3a. I treated the cells with the LY294002 and wortmannin, these PI3K inhibitors induce FoxO3a activation, to clarify whether FoxO3a is involved in melanogenesis [38]. FoxO3a significantly localized in the nucleus when PI3K inhibitors were applied to primary melanocytes (Figure 1d), melanin levels decreased (Figure 1e), and the pigment-related proteins were downregulated, which are tyrosinase (TYR), tyrosinase-related protein 1 (TYRP1), and dopachrome tautomerase (dopachrome delta-isomerase, tyrosine-related protein 2, DCT) (Figure 1f).

I induced FoxO3a siRNAs into MNT1 cells, which are highly pigmented human melanoma cells with mature stage III and IV melanosomes to identify that Foxo3a is a factor in modulation of melanogenesis (Figure 1a). Two different types of FoxO3a-directed siRNAs (si-1 and si-2) were used and confirmed that both were functioning properly by qPCR and immunoblot assay (Figure 2a and c). When siRNAs against FoxO3a were introduced into cells, the expression of melanogenesis-related genes, such as microphthalmia-associated transcription factor (MITF),

tyrosinase-related protein 1 (TYRP1), dopachrome tautomerase (DCT), and tyrosinase (TYR) were upregulated, whereas the expression of stem cell factor (SCF), the SCF receptor (cKit), and SRY-related HMG-box (SOX10), which are associated with cell proliferation rather than melanogenesis were downregulated (Figure 2a-b). Consistent with the pigment-related genes upregulation, the MITF, TYR, TYRP1, and DCT protein levels increased (Figure 2c). In addition, compared with control or mock (negative control siRNA)-treated cells, accumulated levels of melanin (Figure 2d-e) and tyrosinase activity (Figure 2f) were significantly elevated in Foxo3a siRNA-treated cells, indicating that FoxO3a down-regulates pigment-related genes results in melanogenesis inhibition. And hence, I investigated the early to late melanogenesis-related genes expression. By FoxO3a siRNA treatment, the mRNA levels of paired box transcription factor (PAX3), melanoma antigen recognized by T-cells (MART1), endothelin receptor B (EDNRB), and p75NTR were increased compared with the BRN2, S100β, and NOTCH1 levels were downregulated (Figure 3a-b).

FoxO3a nuclear translocation suppress melanogenesis

FoxO3a functions as transcription factor in downstream of the PI3K-PKB (also called AKT) pathway [39]. The activation of PI3K-PKB pathway reduces FoxO3a nuclear translocation by phosphorylation of FoxO3a and its transactivation activity is also suppressed [40,41]. To induce FoxO3a nuclear translocation and activation, I used the well-known PI3K inhibitors LY294002 and wortmannin [38]. The melanin levels decreased by 59% (LY294002) and 60.3% (Wortmannin) when PI3K inhibitors were applied to cells compared with the untreated groups (Figure 4a-b), and the tyrosinase activity was reduced by 57.8% and 54.6%, respectively (Figure 4c). In contrast with the results shown for FoxO3a-directed siRNA expression, mRNA expression levels

of the early stage markers of melanogenesis, such as *cKit, scf, sox10, notch1, and brn2*, were increased and the melanogenesis-related genes *tyrosinase, mitf, tyrp1, dct, pax3,* and *ednrb* were decreased (Figure 3c-d and 4d-e). The mRNA and protein expression levels of FoxO3a were increased by PI3K inhibitors which result in nuclear accumulation of FoxO3a proteins (Figure 4e-f). The protein expression of MITF, TYR, TYRP1, and DCT were downregulated coincide with the nuclear accumulation of FoxO3a, suggesting that the large amount of nuclear FoxO3a inhibit melanogenesis (Figure 4f).

FoxO3a nuclear translocation is a critical event in melanogenesis regulation

As shown above results using FoxO3a siRNA and PI3K inhibitors, FoxO3a expression levels and nuclear localization are important in melanin formation; however, it still remains unclear whether the FoxO3a expression level or localization is more intensively associated with melanogenesis modulation. Therefore I constructed plasmids expressing wild-type FoxO3a (plasmid 1787: HA-FoxO3a; WT) or deletion mutant in the nuclear localization sequence (NLS), a mandatory region for FoxO3a translocation [42] (plasmid 8361: FLAG-FoxO3a TM; ΔNLS) to investigate the effect on melanogenesis of FoxO3a nuclear translocation. The total level of FoxO3a proteins largely increased under both of the wild-type or mutant constructs transfection conditions (Figure 4g, lower panel, whole FoxO3a), whereas only under the wild-type over-expression condition, the nuclear FoxO3a levels were increased (Figure 4g, upper panel). Moreover in the wild-type-expressing cells but not the NLS mutant-expressing cells, the melanin levels largely decreased (Figure 4h), suggesting that the nuclear translocation is more closely associated with melanogenesis rather than the Foxo3a protein levels. Nuclear translocation of FoxO3a results in its activation [12]. In this regards, FoxO3a regulates melanogenesis by its activation via nuclear

translocation. I next evaluated Akt-directed siRNA or an Akt inhibitor for Akt inhibition to clarify that FoxO3a nuclear translocation is the essential factor for regulation of melanogenesis. Transfection with FoxO3a-directed siRNA increased melanin production by 114.8%, whereas treatment Akt siRNA or Akt inhibitor decreased melanin by 61.7% and 59%, respectively (Figure 4i). The inhibition of Akt blocked phosphorylation of FoxO3a (Figure 4j), and FoxO3a nuclear translocation was greatly increased (Figure 4k). According to these results, I suggest that nuclear translocation of FoxO3a by either PI3K or Akt inhibition induces the repression of melanogenesis.

Anti-melanogenic activity of antioxidants are mediated by FoxO3a activation

Many antioxidants have been used to treat skin hyperpigmentation because enzymatic oxidation steps occur during melanin synthesis. Vitamin C (Vc), vitamin E, hydroquinone, and N-acetylcysteine (NAC) have been generally used to decrease melanin levels, and synergetic effects of antioxidants have been shown [43,44]. However, the mechanism of melanogenesis regulation by antioxidants has not yet been explored in detail. I first investigated the effects of antioxidants on pigmentation, including vitamin C, NAC, and Trolox (a water-soluble derivative of vitamin E) to reveal this mechanism. As previously reported [43] under certain degree of antioxidant, the melanin levels and tyrosinase activity gradually decreased. On the other side, these effects were transient, and under concentrations higher than 100 nM, antioxidant treatment induced increasing the melanin levels and tyrosinase activity gradually (Figure 5a). Despite of their different structure and ROS scavenging activity, antioxidants showed similar inhibition patterns against melanin formation. A tyrosinase activity, cell cytotoxicity, and proliferation were not impacted by each antioxidant in experimental concentration extent (Figure 6). The mRNA and protein levels of

tyrosinase and DCT were markedly reduced with 100 nM antioxidant treatment meanwhile, the expression of MITF and TYRP1 remained unchanged (Figure 5b-c).

In the aging model organism *C. elegans*, antioxidants induce the nuclear translocation of DAF-16 (a homolog of Foxo3a) [37]. I speculated that anti-melanogenic effects of antioxidants triggered by FoxO3a nuclear translocation and activation. To confirm my hypothesis, I performed immunofluorescence assays for observing FoxO3a localization. The FoxO3a nuclear translocation by each antioxidant (Vc, NAC, and Trolox) displayed gradual enrichment up to 100 nM and a gradual reduction at greater concentrations (Figure 7). I presented that 100 nM of each antioxidant showed the greatest anti-melanogenic activity and also the nuclear localization of FoxO3a which was the concentration that yielded (Figure 8a). These results indicate that Foxo3a nuclear translocation by antioxidant modulate melanogenesis. Endogenous nuclear FoxO3a was enriched in antioxidant-treat cells without a change in the total protein levels (Figure 8b-c). Next, I performed a time-course experiment for FoxO3a nuclear translocation. FoxO3a translocalized to the nucleus by Vc after 2 hours and gradually accumulated with time (Figure 8d). FoxO3a nuclear localization is continuous rather than transient and this process arises directly and quickly (Figure 8d). Whereas antioxidants induced nuclear translocation of Foxo3a, another FoxO protein, FoxO1 translocation did not observed (Figure 9).

I pretreated FoxO3a-direct siRNA in MNT1 cells and then applied each antioxidant to certify that the FoxO3a activation induces anti-melanogenic effect of antioxidants. FoxO3a siRNA induces increasing tyrosinase activity and melanin formation (Figure 10a-c). And as expected, increased tyrosinase activity and melanin levels did not reversed by any antioxidant treatment (Figure 10a-c) at any dose (Figure 10d). Same as these results, increased melanogenesis did not reduced also by PI3K inhibitor treatment (Figure 10e). Even though certain doses of antioxidants

and wortmannin reduced the FoxO3a siRNA-induced melanin, these were not characteristic degrees. These results suggest that antioxidants produce anti-melanogenic effects by FoxO3a pathway mediation.

SYR attenuates age-related skin atrophy and oxidative damage in *Sod1*$^{-/-}$ mice

In *Sod1*$^{-/-}$ mice, skin thickness was prominently decreased compared with wild-type mice [19]. Oral treatment with ginseng berry extract (GB) and its bioactive component SYR significantly increased skin thicknesses in hairless *Sod1*$^{-/-}$ mice compared with vehicle-treated *Sod1*$^{-/-}$ mice (Figure 11a, 11b, and 12). The attenuation of age-related skin atrophy was remarkable, especially in the dermis. SYR or GB treatment was performed from 6 weeks of age or 16 weeks of age for 8 weeks. In both conditions, SYR effectively recovered age-related skin atrophy (Figure 11a, 11b, and 13), as well as GB (Figure 13 and 14). I also observed the dose-dependent manner of SYR and GB in skin thinning at 14-week-old *Sod1*$^{-/-}$ mice (Figure 13 and 14). These findings demonstrated that SYR *p.o.* treatment significantly improved skin atrophy of hairless *Sod1*$^{-/-}$ mice, particularly in the dermis. Because *Sod1*$^{-/-}$ mice show increased oxidative damage compared with wild-type mice, I measured the levels of oxidative damage markers and intracellular ROS in the skin region. As expected, SYR administration lowered the levels of lipid peroxide marker 8-isoprostane in the skin (Figure 11c) and DCF intensity as intracellular ROS in cultured primary fibroblasts (Figure 11d). Next, I investigated the protective effects of SYR against skin damage. Organ culture experiments using skin discs demonstrated a markedly lower outgrowth capacity in *Sod1*$^{-/-}$ fibroblasts compared with that in *Sod1*$^{+/+}$ fibroblasts, indicating that the migration and proliferation of the *Sod1*$^{-/-}$ fibroblasts were impaired (Figure 11e). To analyze the protective effects of SYR, I next added SYR to cultures of *Sod1*$^{-/-}$ skin discs. Although SYR

treatment did not induce any significant changes in *Sod1*$^{+/+}$ skin, SYR significantly promoted the fibroblast outgrowth capacity in *Sod1*$^{-/-}$ skin discs (Figure 11e). These findings demonstrated that the application of SYR ameliorated both skin atrophy and oxidative damage in *Sod1*$^{-/-}$ mice.

SYR does not activate collagen synthesis through NF-κB signaling

In a previous study, I showed that ginsenoside Re from GB inhibit the transcription factor v-rel reticuloendotheliosis viral oncogene homolog A (RelA, also known as NF-κB p65), thus activating collagen synthesis [45]. Because SYR is also derived from GB, I investigated whether SYR treatment affects NF-κB signaling and procollagen expression. However, SYR treatment did not inhibit the elevated phosphorylation of NF-κB in *Sod1*$^{-/-}$ mice (Figure 15a). In addition, SYR treatment did not activate the transcription of procollagen 1a1/*Col1a1* (Figure 15b) and did not suppress the expression of inflammatory cytokine interleukin-6/*Il-6* (Figure 15c), both of which were regulated by NF-κB. These results indicated that the protective effects of SYR against age-related skin atrophy were independent of the NF-κB signaling pathway.

SYR inhibits MMP-2 expression via FoxO3a dephosphorylation

Since SYR did not affect collagen synthesis, I explored other pathways that might prevent the skin aging process. In my previous work using a human MNT1 melanoma cell line, SYR displayed potent antioxidative activity and inhibited skin melanogenesis by activating the forkhead box O protein, FoxO3a [46]. I previously reported that antioxidants induce FoxO3a nuclear localization by inhibiting its phosphorylation, which results in its activation [47]. Therefore, I hypothesized that SYR also promotes FoxO3a dephosphorylation *in vivo*. FoxO3a phosphorylation was elevated in *Sod1*$^{-/-}$ mice, indicating that both FoxO3a nuclear export and

activation were inhibited, although total expression of FoxO3a was not changed significantly (Figure 15a). According to my results, SYR-treated mice had greatly reduced FoxO3a phosphorylation compared with vehicle-treated and *Sod1*$^{+/+}$ mice (Figure 16a). Then, I investigated phosphorylated FoxO3a (p-FoxO3a) levels in mouse skin via immunohistochemistry. Interestingly, I confirmed that dermal thickness was recovered and that p-FoxO3a expression was greatly repressed in *Sod1*$^{-/-}$ mouse skin following SYR treatment (Figure 15d and 17). Although the expression of the SIRT1, which was a FoxO3a downstream-related protein, was not markedly changed (Figure 18), SYR treatment clearly inhibited FoxO3a phosphorylation in mouse skin (Figures 15a, 15d, and 17). During skin aging, collagen degradation by collagenase is a major factor in the decline of skin thickness. Previously, I observed the significant upregulation of matrix metalloproteinase-2 (MMP-2), which was a member of the type IV collagenase, in *Sod1*$^{-/-}$ skin [24], while others indicated that FoxO3a directly down-regulates MMP-2 expression in vascular smooth muscle cells [48]. Therefore, I hypothesized that SYR-induced FoxO3a dephosphorylation affects MMP-2 expression and rescues age-related skin atrophy. I investigated MMP-1 and MMP-2 expression in mouse skin via immunohistochemistry. Expectedly, MMP-2 expression decreased dramatically after SYR treatment (Figure 16a). To confirm this result, I also investigated the protein and mRNA expression levels of these proteins in mouse back skin. MMP-1 and MMP-2 protein expression was elevated in *Sod1*$^{-/-}$ mice compared with wild-type mice. Intriguingly, only MMP-2 expression was greatly suppressed by SYR treatment (Figure 16b and 16c), similar to the immunohistochemistry data. Additionally, qRT-PCR analysis also revealed a similar pattern as the above data (Figure 16d). Here, I also displayed the immunohistochemistry data on MMP-2 expression levels from GB-treated *Sod1*$^{-/-}$ mice (Figure 19). According to these data, SYR and GB treatment strongly abrogated MMP-2 expression,

which was elevated by aging-like processes in mice. These data indicates that SYR treatment rescues age-related skin atrophy by inhibiting MMP-2 expression, which is mediated by FoxO3a dephosphorylation.

Discussion

Melanin formation steps include enzymatic oxidation steps in the melanin polymer syntheses and engagement. In this regards, many antioxidative reagents have been used to skin hyperpigmentation; however, the modulatory mechanism is not clarify in detail. FoxO3a, well-known anti-aging transcription factor, controls many target genes that are involved in the antioxidative response in diverse cell types, including skin cells. In this study, I propose that FoxO3a is a novel anti-melanogenic factor by involving melanogenesis regulation. Based on my results from FoxO3a knockdown, overexpression and the activation using PI3K inhibitors and Akt inhibition, I suggest that FoxO3a is an anti-melanogenic factor. I also demonstrated that antioxidants induce anti-melanogenic activity by FoxO3a nuclear translocation, result in its activation.

Anti-melanogenic effect of antioxidants is simply explained by reduced cellular ROS level by its ROS scavenging effect. However, melanin synthesis inhibition by antioxidants was not dose-dependent event. According to my results, FoxO3a activation by antioxidants has good coordination with its anti-melanogenic effect (Figure 8 and 10), giving a reasonable molecular mechanism. I detected that the tyrosinase activity and also melanin levels were reduced to a certain extent in response to antioxidant treatments; the maximum efficacy was presented at 100 nM, and higher doses showed lowered effects. These anti-melanogenic effects were well coordinated with the FoxO3a nuclear translocation (Figure 5 and 7-8). Hermetic (bell-shaped or U-shaped) concentration efficacy curves are often observed for many chemicals, including drugs, toxins, oxidants, and antioxidants [49]. FoxOs are assumed as key players in redox signaling because they transcript ROS-scavenging enzymes and, adversely, its activities are post-translationally regulated by oxidative stress [50]. As previously reported, the FoxO cysteine

residues have been reported to be involved in the interaction with nuclear import receptor transportin-1 through disulfide formation and act as sensors for the local redox state. The nuclear translocation of FoxO regulated through varying stability and interaction aspect induced by different redox states [51]. This finding may give a hint about concentration higher than 100 nM rather reduce FoxO3a nuclear translocation. The reduced anti-melanogenic effects of antioxidant at high concentrations may explained by cellular defense mechanisms against hyper-reductive conditions. After sensing a hyper-reductive state for the oxidative and reductive states balance, then cells activate a re-oxidation signaling evoked by the FoxO protein. A hyper-reductive state inside cells was induced by high levels of antioxidants, and then reduces FoxO nuclear translocation by which inhibitions disulfide formation with binding partners.

FoxO3a overexpression or activation affected the expression of melanogenesis-related genes, MITF, tyrosinase, TYRP-1, and DCT (Figure 4). On the other hand, FoxO3a activation by antioxidants seems to selectively affect the expression of tyrosinase and DCT among them (Figure 5). Furthermore, antioxidants and PI3K inhibitors could not recover the elevated melanin synthesis caused by the FoxO3a siRNA pre-treatment (Figure 10). These results indicate that FoxO3a pathway is a key factor for modulation of melanogenesis-related genes by antioxidant-mediated melanogenesis regulation.

In my study, FoxO3a was proven to be an essential factor for the melanogenesis regulation. There are still many of unsolved questions remains unknown such as the mechanism by which FoxO3a regulates many melanogenic genes. Generally, many proteins exist which interacts and forms a complex with FoxO3a, there is a possibility of binding and generating high molecular weight complexes and perform functions that are associated with melanogenesis in the nucleus. The FoxOs contain one forkhead-binding domain fused with the transcriptional activation

domain. FoxOs generate a chimeric form by interaction with forkhead-binding domain and the DNA-binding domain of other transcription factors [52]. In the previous study, the PAX3-FoxO1 chimeric form has been found in alveolar rhabdomyosarcoma and consists of the transactivation and DNA-binding domains of FoxO1 and PAX3, respectively [53], suggesting that FoxO3a may also interact with PAX3. Peroxisome proliferator-activated receptor (PPAR) gamma coactivator (PGC)-1α could be another possible binding target of FoxO3a. PGC-1α is regulated by alpha-melanocyte stimulating hormone (α-MSH) and activates MITF in human melanoma cell lines [54]. According to previous report, FoxOs regulate PGC-1α transcriptionally and post-translationally and they can co-operate with each other [55]. In my results, PAX3 and MITF mRNA levels upregulated by deletion of FoxO3a using siRNA and FoxO3a activation by PI3K inhibitors reversed this effect. Considering my results, PAX3 and PGC-1α do not seem to be direct transcriptional binding targets of FoxO3a. However, these melanogenic factors still have potential for FoxO3a binding partners in melanogenesis modulation. I also suppose that other melanogenesis-related proteins, such as SCF, cKit, and SOX10, for which their expression levels were influenced with FoxO3a modulation, could be transcriptional targets of FoxO3a.

In skin hyperpigmentation and melanoma, operating ROS production or the activity of cellular regulators has been thought as an attractive therapeutic target for inhibiting melanogenesis. Typically, in order to reduce melanin synthesis, pharmacological agents primarily focused on eliminating ROS via the antioxidative process. Based on my present study, an anti-melanogenic effect of antioxidants mediates FoxO3a. Because FoxO3a is related with longevity in many aging model organisms, this study suggests that FoxO3 could be a potent target for tracing both anti-aging and anti-melanogenic effects.

The age-related phenotype of senescence involves the attenuation of various organs. SOD1

reacts with intracellular O_2^- in the cytoplasm. *Sod1*$^{-/-}$ mice exhibit various age-related organ phenotypes because of increased intracellular O_2^- concentrations. Oxidative damage is among the major factors underlying senescence-related changes in various tissues and organs. In addition, *Sod1* incompetence results in skin atrophy, which is associated with the decrease in extracellular matrix related-genes, such as *Col1a1* and *Has2* [24]. Therefore, *Sod1*$^{-/-}$ mice constitute a suitable model for studying age-associated skin aging. Recently, I further established hairless *Sod1*$^{-/-}$ double-mutant mice to avoid variations in skin morphology during the hair cycle [32]. Thus, these double-mutant mice will be a valuable mouse model for mimicking age-related skin thinning. In this context, the present study explored the feasibility of using natural antioxidant treatment to delay skin aging. I investigated the beneficial effects of *Panax ginseng* berry, which contains several bioactive compounds [56-59], as well as its bioactive compound SYR, on hairless *Sod1*-deficient phenotypes.

Among the senescence phenotypes of tissues, skin undergoes marked changes during aging. With senescence, the thickness of both the dermis and epidermis decrease considerably. In *Sod1*$^{-/-}$ mice, the thickness of the dermis was markedly decreased (Figure 11a and Figure 12-14). The attenuating effects of GB or SYR on skin atrophy were mediated by its antioxidative activity. SYR treatment reduced the levels of an oxidative stress marker and intracellular ROS (Figure 11c, d). Because SYR activated fibroblast proliferation (Figure 11e) and given previous reports that ginseng extracts inhibit NF-κB signaling [45], I hypothesized that SYR also induces this signaling pathway. However, SYR did not affect NF-κB phosphorylation or procollagen expression (Figure 15a, b). Since collagen synthesis is a major factor in skin aging, SYR likely affects another pathway that regulates collagen homeostasis.

Class O forkhead/winged helix (FoxO) transcription factors are critical regulatory factors of

various biological events, including metabolism, growth, development, and longevity [60,61]. FoxO factors are involved in cellular signaling and are activated by various environmental stimuli such as insulin, insulin growth factors (IGFs), oxidative stress, cytokines, and nutrients. In particular, oxidative stress inhibits or activates FoxO factors in a context-dependent manner. For instance, hydrogen peroxide inhibits FoxO activity by activating the phosphoinositide 3 kinase-protein kinase B pathway by exhibiting insulin-mimetic effects [15], whereas ROS-activated macrophage-stimulating 1, mitogen-activated protein kinase, and c-Jun N-terminal kinase activate FoxO via phosphorylation and by disrupting 14-3-3 binding [16,17]. In skin, FoxO3a down-regulation promotes cellular senescence in human dermal fibroblasts [62]. In addition, FoxO3a regulates UVB protection, and its nuclear translocation is also regulated by UV irradiation [63,64]. These studies suggest that FoxO3a plays an important role in cellular responses in the skin that are induced by external stimulation. In addition, previous reports suggest that reduced FoxO3a expression results in low autophagy in fibroblasts grown on a collagen matrix [65] and that FoxO3a promotes fibroblast proliferation on a type I collagen matrix [66]. my previous studies indicated that SYR activates FoxO3a in cardiomyocytes [67], as well as in skin cells, fibroblasts and melanocytes. Therefore, I predict that the activation of FoxO3a by SYR results in the activation of collagen synthesis or the inhibition of degradation. Previously, Wang *et al*. reported that FoxO3a down-regulates MMP-2 in smooth muscle cells [48]. Initially, I examined whether FoxO3a phosphorylation was reduced in the SYR-treated group (Figure 15a, d and Figure 17). Then, I investigated MMP-1 and MMP-2 protein expression in mouse back skin. Interestingly, SYR strongly suppressed MMP-2 upregulation in *Sod1*$^{-/-}$ mice but did not affect MMP-1 expression (Figure 16 and Figure 19). To uncover the molecular mechanism of SYR, I performed examined the expression of MMP-2 under w/o siFoxO3a condition in gene and protein level. The *mmp-2*

gene expression was decreased by SYR treatment in Human dermal fibroblasts (HDFs) about 41% however in siFoxO3a condition, SYR did not lowered *mmp-2* expression significantly. SYR also declined MMP-2 protein expression and gelatinase activity about 60% and 51.8% respectively, in FoxO3a-dependent manner (Figure 20). Although these results did not explain molecular mechanism of SYR clearly, I suggest that the anti-aging effects of SYR in skin largely affected by FoxO3a activation.

In conclusion, SYR treatment attenuates senescence-related skin atrophy in *Sod1*$^{-/-}$ mice via FoxO3a activation. Activated FoxO3a results in the inhibition of collagen degradation by somehow suppressing MMP-2 expression. my results suggest that *Sod1*$^{-/-}$ mice are a good model for studying age-related skin atrophy and that skin aging can be prevented by natural compounds. my findings imply that modulation of signaling for FoxO3a-mediated collagen biosynthesis, which is not yet fully defined, and that the use of FoxO3a activators may help prevent skin senescence. Overall, these studies suggest that FoxO3a activation may be a novel therapeutic strategy for the treatment and prevention of dermal aging.

Materials and Methods

Materials and administration

MITF (C5), tyrosinase (H-109), TYRP-1 (H-90), DCT (C-9), GAPDH (FL-335), and Lamin B (C-5) antibodies were purchased from Santa Cruz Biotechnology. Antibodies against MITF (Noemarkers, Fremont, CA) and tyrosinase (Upstate biotechnology, Lake Placid, NY) were also used. FoxO3a (#9467), FoxO3a (75D8), FoxO1 (C29H4), FoxO4 (55D4), phospho-FoxO3a (#9466), Akt (#9272), and phosphor-Akt (#4060) antibodies were obtained from Cell Signaling Technology. The PI3K inhibitors LY294002 and wortmannin were obtained from Cell Signaling Technology. Akt inhibitor 1/2 (A6730) was purchased from Sigma. Secondary antibodies for western blot and immunofluorescence were obtained from Cell Signaling Technology and Invitrogen, respectively. Plasmids for HA-FoxO3a WT (1787) and NLS mutant, FLAG-FoxO3a TM (8361) were obtained from Addgene. FoxO3a validated stealth RNAi duopak and scramble RNAi were purchased from Invitrogen.

[8R,8'R]-[+]-syringaresinol (HanChem Co., Ltd., Daejeon, Korea) or ginseng berry extract (provided by R&D Center of Amorepacific Corporation, Yongin, Korea, Lot number 1305) were suspended in MilliQ water. For the first trial, SYR (10 or 50 mg/kg/day) or ginseng berry extract (100 or 300 mg/kg/day) were administered orally via gavage to hairless *Sod1*$^{-/-}$ mice (n = 11-13) at 6 weeks of age for 8 weeks. For the second trial, SYR (50 mg/kg/day) or ginseng berry extract (300 mg/kg/day) were administered orally via gavage to hairless *Sod1*$^{-/-}$ mice (n = 8-10) at 16 weeks of age for 8 weeks.

Animals

Hairless *Sod1*$^{-/-}$ double-mutant mice constitute a valuable mouse model for mimicking age-

related skin thinning [24]. *Sod1*$^{-/-}$ mice were purchased from the Jackson Laboratory (Bar Harbor, ME, USA) and backcrossed with C57BL/6NCrSlc mice (Japan SLC, Shizuoka, Japan) over ten generations. Hos:*HR-1*$^{hr/hr}$ mice were purchased from Hoshino Laboratory Animals, Inc. (Ibaraki, Japan), and hairless *Sod1*$^{-/-}$ double-mutant mice were generated by crossbreeding Hos:*HR-1*$^{hr/hr}$ with *Sod1*$^{-/-}$ mice for five or six generations. *In vivo* analyses were performed using *in vitro* fertilization and embryonic transfer techniques to generate hairless *Sod1*$^{-/-}$ and hairless *Sod1*$^{+/+}$ male mice. Genotyping of the *Sod1*$^{-/-}$ allele was performed using genomic PCR with genomic DNA biopsied from the tail tips of mice at 3-4 weeks of age. The animals were housed under a 12 h light/dark cycle and fed *ad libitum* MF chow (Oriental Yeast Co., Ltd., Tokyo, Japan). Male mice were separated from female mice at 3 weeks of age, and the housed cages were divided into groups based on the average body weights at one week before administration. The mice were maintained and studied according to protocols approved by the Animal Care Committee of Chiba University.

Cell culture and growth activity assay

MNT1 cells were maintained in Minimum Essential Media (Gibco) containing 10% Dulbecco's Modified Eagle's Medium, 20 mM HEPES (Sigma), 20% fetal bovine serum, 100 U/mL penicillin G, and 100 μg/mL streptomycin sulfate. MNT1 cells were incubated at 37℃ with 5% CO_2 and regularly passaged at a density of 80% (1:8 ratio). Dermal fibroblasts from adult skin were purchased from Lonza (Walkersville, MD, USA) and maintained in DMEM supplemented with 1% penicillin/streptomycin and 10% heat-inactivated fetal bovine serum (FBS, Gibco, Carlsbad, CA, USA). The cells were cultured and regularly passaged at a density of 90% confluent. Cell proliferation and cytotoxicity were measured using cell counting kit-8 (Dojindo,

Japan).

Antioxidant activity assay

The catalase activity was determined from the amount of the residual H_2O_2 as measured by a spectrophotometric method. Briefly, 800 μL of 25 μM H_2O_2 and 200 μL of a sample solution in water that contained ginseng root extract, ginseng berry extract or syringaresinol were added to initiate the quenching reaction. After five min incubation, the concentration of H_2O_2 was measured at 240 nm. Water was used as a vehicle control, and the residual H_2O_2 is represented as a percentage of the control.

The DPPH (1,1-diphenyl-2-picrylhydrazyl) radical scavenging activity was calculated from the residual DPPH concentration, as estimated by a spectrophotometric method (Yamazaki et al., 1994). In brief, 500 μL of 60 μM DPPH was placed in a quartz cuvette, and same volume of a sample solution in ethanol that contained ginseng root extract, ginseng berry extract or syringaresinol were added to initiate the DPPH quenching. The quenching reaction was performed for thirty min incubation at room temperature (RT) and absorbance at 520 nm was measured using spectrometer. The residual DPPH is expressed as a percentage of the control and ethanol was used as a vehicle control.

Tyrosinase enzymatic activity assay and determination of melanin levels

To assess cellular tyrosinase activity, equal amounts of cell lysates (10 μg) were incubated with 10 mM L-dihydroxyphenylalanine (L-DOPA) (pH 6.8) at 37℃ for 1 h. Melanin synthesized from L-DOPA by tyrosinase in the cell extracts was measured at 490 nm in a UV-Vis

spectrometer (Molecular Devices). Mushroom tyrosinase catalytic activity was measured by incubating 2 mg/mL mushroom tyrosinase (Sigma) with 10 mM L-DOPA solution supplemented with the reagents of interest at 37℃ for 1 h. Melanin levels were measured at 490 nm. To measure cellular melanin levels, the cell pellets were dissolved in 1 N sodium hydroxide, and melanin levels were determined by measuring the absorbance at 490 nm. The melanin levels were normalized to protein input.

Small interfering RNA and plasmid transfection

MNT1 cells cultured in 60 mm dishes were transfected with stealth RNAi duopak FoxO3a (CAT No. 45-1712, Invitrogen), SignalSilence Akt siRNA (#6211, Cell Signaling Technology), and a Stealth RNAi^{TM} siRNA negative control kit (CAT No. 12935-100, Invitrogen) using Lipofectamine^{TM} RNAi MAX (Invitrogen) and 5 nM siRNA for 48 h, according to the manufacturer's instructions. MNT1 cells (3.5×10^5 cells/6 wells) were grown to 60-70% confluence and then transfected with 4 μg of plasmid. The plasmids included constitutively active HA-FoxO (1787, Addgene) and constitutively active FoxO3a NLS mutant, FLAG-FoxO3a TM (8367, Addgene).

FoxO localization assay using immunofluorescence

MNT1 cells were treated with each reagent (Vc, NAC, and Trolox) for 4 days, washed with PBS, fixed for 30 min in 4% paraformaldehyde, washed again, and incubated for 10 min in 0.1% Triton X-100. The cells were washed three times in PBS and incubated with anti-FoxO3a (1:200) or anti-FoxO1 antibodies (1:200) diluted in Hank's solution (0.44 mM KH_2PO_4, 5.37 mM KCl, 0.34 mM Na_2HPO_4, 136.89 mM NaCl, and 5.55 mM D-glucose) at 4°C overnight. Secondary

antibodies (Alexa Fluor 555- or Alexa Fluor 488-conjugated goat anti-rabbit or -mouse) were added for 1 h at room temperature. After washing, the coverslips were mounted onto glass slides and visualized using an EVOSfl digital fluorescence microscope (Advanced Microscopy Group) (Ex: 555 nm; Em: 565 nm for FoxO3a, Ex: 488 nm; Em: 519 nm for FoxO1).

Cellular fractionation assay

Cytoplasmic and nuclear fractions were prepared according to a previously published protocol (Schreiber *et al*., 1989). Briefly, the cells were lysed in a cytosolic lysis buffer containing 10 mM HEPES (pH 7.9), 10 mM KCl, 0.1 mM EGTA, 0.1 mM EDTA, 10% NP-40, 0.5 mM PMSF, 1 mM DTT, and protease inhibitors. The nuclei were pelleted via a short centrifugation step and lysed in a nuclear buffer containing 20 mM HEPES (pH 7.9), 400 mM NaCl, 1 mM EGTA, 1 mM EDTA, 1 mM PMS, 1 mM DTT, and protease inhibitors. The nuclear pellets were subjected to three freeze-thaw cycles before they were sonicated and centrifuged to obtain a solubilized nuclear fraction.

Western blot analysis

MNT1 cells were lysed in lysis buffer containing 20 mM Tris-HCl (pH 7.5), 150 mM NaCl, 1 mM DTT, 0.5% NP-40, 25 mM β-glycerophosphate, 1 mM sodium orthovanadate, 0.5 mM PMSF, and a protease inhibitor cocktail (Protease inhibitor, Sigma) and incubated with the appropriate antibodies for 1 h. This incubation was followed by the addition of pre-cleared protein G beads (GE Healthcare) overnight at 4℃. Next, the beads were washed five times with lysis buffer. Western blotting was performed following standard protocols. The cell lysates (20 μg protein) were boiled in SDS sample buffer and resolved using 4-12% SDS-PAGE. The

proteins were then transferred to a PVDF membrane (Invitrogen) and probed using specific antibodies.

Mouse skin tissues were homogenized in 5 volumes (w/v) of RIPA buffer (25 mM Tris-HCl, pH 7.5, 150 mM NaCl, 1% NP-40, 1% sodium deoxycholate, and 0.1% sodium dodecylsulfate) supplemented with protease and phosphatase inhibitor cocktails (Roche Diagnostics, Tokyo, Japan). The protein concentrations of the homogenates were determined using the DC Protein Assay Kit. Proteins (20-40 μg/lane) were separated on a 6.5-10% polyacrylamide gel with Laemmli buffer and transferred to a PVDF membrane (0.4 μm pore size, Immobilon-P, Millipore, Germany) using a Transblot Turbo (Bio-Rad, Hercules, CA, USA) with Rapid Transfer buffer (Amresco, Solon, OH, USA, N789, 25 V for 30 min) for total FoxO3a or with Towbin buffer (25 mM Tris, 192 mM glycine) without methanol (20 V for 40 min or 25 V for 30 min) for other proteins. For the detection of transcription factors, the membrane was blocked with 3% bovine serum albumin (Nacalai Tesque, Kyoto, Japan) in TBST (TBS containing 0.01% Tween-20) for 1 h at room temperature. The membrane was blocked with 5% skim milk for all other proteins. The following primary antibodies were used overnight at 4℃: anti-MMP-1 (Abbiotech, CA, USA, #250750 dilution factor 1:200), anti-MMP-2 (Novus Biologicals, CO, USA, NB200-193 dilution factor 1:1000), anti-FoxO3A [75D8] (Cell Signaling, Tokyo, Japan, #2497 dilution factor 1:100), anti-phosphorylated FoxO3A [EPR1951(2)] (Abcam, MA, USA, ab154786 dilution factor 1:500), anti-NF-κB/p65 [D14E12] (Cell Signaling, #8242 dilution factor 1:500), anti-phosphorylated NF-κB/p65 [93H1] (Cell Signaling, #3033 dilution factor 1:500), anti-α-tubulin (Cell Signaling, #2144 dilution factor 1:1000), and anti-GAPDH [14C10] (Cell Signaling, #2118 dilution factor 1:1000). The membrane was then treated with secondary antibody (Cell Signaling, #7074 dilution factor 1:2000) and Clarity Western ECL (Bio-Rad, #1705060) at room temperature

according to the manufacturer's protocols, followed by detection using an LAS-3000 (Fujifilm, Tokyo, Japan).

RT-qPCR

MNT1 cells were homogenized in TRIzol reagent (Gibco), and total RNA was extracted according to a standard protocol. Total RNA (4 μg) was reverse-transcribed using random hexamers and SuperScript III (Invitrogen) according to the manufacturer's instructions. Quantitative PCR was performed using the ABI 7500 Fast Real-Time PCR System with Taqman Universal Master Mix II (Applied Biosystems) and TaqMan site-specific primers and probes (Applied Biosystems). I used the $\Delta\Delta C_T$ analysis method [68]; the efficiency of the target and the reference amplification were approximately equal. Reactions were performed in triplicate and mRNA expression levels were quantified using the relative C_T method and normalized to *GAPDH* level.

Total RNA was extracted from back skin using the RNA*later* and the TRIzol reagent (Thermo Fisher Scientific, Carlsbad, CA, USA) according to the manufacturer's instructions [19]. cDNA was synthesized from 1 μg of total RNA using ReverTra Ace qPCR RT Master Mix (Toyobo, Osaka, Japan). Real-time PCR was performed on a MiniOpticon (Bio-Rad) with the SsoAdvanced SYBR Green Supermix (Bio-Rad) according to the manufacturer's protocols. All data were normalized to the level of the housekeeping gene glyceraldehyde-3-phosphate dehydrogenase (*Gapdh*) or ribosomal RNA 18S (*Rn18S*). The following primers were used for the analysis: *Gapdh*, forward, 5'-ATG TGT CCG TCG TGG ATC TGA-3', and reverse, 5'-TGC CTG CTT CAC CAC CTT CT-3'; *Col1a1*, forward, 5'-CAT GTT CAG CTT TGT GGA CCT-3', and reverse, 5'- GCA GCT GAC TTC AGG GAT GT-3'; *Mmp-1a*, forward, 5'-TGT GTT TCA

CAA CGG AGA CC-3', and reverse, 5'-GCC CAA GTT GTA GTA GTT TTC CA-3'; *Mmp-2*, forward, 5'-TAA CCT GGA TGC CGT CGT-3', and reverse, 5'-TTC AGG TAA TAA GCA CCC TTG AA-3'; *Il-6*, forward, 5'-GCT ACC AAA CTG GAT ATA ATC AGG A-3', and reverse, 5'-CCA GGT AGC TAT GGT ACT CCA GAA-3'; *Rn18S*, forward, 5'-GTA ACC CGT TGA ACC CCA TT-3', and reverse, 5'-CCA TCC AAT CGG TAG TAG CG-3'; and *Sirt1*, forward, 5'-CAG TGA GAA AAT GCT GGC CTA-3', and reverse, 5'-TTG GTG GTA CAA ACA GGT ATT GA-3'.

Lipofuscin accumulation

Dermal fibroblasts from adult skin were cultured with each reagent for 10 passages (3-4 days per 1 passage), washed with PBS, and fixed in 4% paraformaldehyde for 30 min. The cells were then washed and incubated in 0.1% Triton X-100 for 10 min. After washing, the cover slips were mounted onto glass slides and visualized by a confocal laser scanning microscope (LSM7, Carl Zeiss) (with an excitation wavelength at 350 nm and an emission wavelength at 420 nm). The fluorescence intensities of the cells were measured densitometrically with the ZEN Lite software (Carl Zeiss) by calculating the average pixel intensity in each cell. The significance of the differences among the control and experimental groups were analyzed using a one-way ANOVA.

Histology

For histological observations, skin specimens obtained from the backs of the mice were dissected and fixed overnight in a 20% formalin neutral buffer solution (Wako, Osaka, Japan). Then, the specimens were embedded in paraffin and sectioned on a microtome at a thickness of 4 μm using standard techniques [24]. Skin tissue thickness (epidermis and dermis) was measured in

hematoxylin and eosin-stained sections using the Leica QWin V3 imaging software program (Leica, Germany). For immunohistochemistry, deparaffinized sections were autoclaved at 95℃ in 10 mM citric acid and 0.05% Tween 20, pH 6.0, for 30 min and then treated with 3% H_2O_2 in PBS(-) at room temperature for 30 min. After being blocked with 3% goat serum in PBS(-), the sections were incubated overnight at 4℃ with anti-MMP-1 (Abbiotech, CA, USA, #250750 dilution factor 1:300), anti-MMP-2 (Novus Biologicals, CO, USA, NB200-193 dilution factor 1:300), and anti-phosphorylated FoxO3A (Abcam, MA, USA, ab154786 dilution factor 1:50) antibodies. Immunoreactivity was visualized using a VECTASTAIN ABC Elite kit (Vector Laboratories, CA, USA) with biotinylated anti-rabbit antibody according to the manufacturer's protocols, followed by staining with 0.05% diaminobenzidine, 50 mM Tris-HCl, and 0.1% H_2O_2, pH 7.5. The sections were counterstained with Meire's hematoxylin (Wako, Osaka, Japan).

Measurement of oxidative stress markers

To measure 8-isoprostane content, blood was collected from the left ventricular space into EDTA-coated collection tubes (Terumo, Tokyo, Japan) and centrifuged at 6,000 rpm for 5 min at room temperature. Plasma was separated from clotted blood and added to 100 μM indomethacin and 50 μg/ml dibutylhydroxytoluene (BHT, Wako). The back skin tissues of male mice were homogenized with 0.1 M phosphate buffer, pH 7.4, containing 1 mM EDTA (Dojindo Laboratories, Kumamoto, Japan) and 50 μg/ml BHT. The homogenate was centrifuged at 8,000 × g for 10 min at 4°C, and the total supernatant was used for the assay. The 8-isoprostane level was measured using the 8-isoprostane EIA Kit (Cayman Chemical Company, Arbor, MI, USA) according to the manufacturer's instructions. The skin supernatant was also assayed for the protein concentration using the DC Protein Assay Kit (Bio-Rad, Hercules, CA, USA), and 8-

isoprostane levels were normalized to protein levels. For measuring of the intracellular ROS, skin tissues were dissected from *Sod1*$^{+/+}$ and *Sod1*$^{-/-}$ mouse neonates at 5 days of age. Primary dermal fibroblasts were isolated by dissociation in 0.2% collagenase type 2 (Worthington Biochemical Corporation Lakewood, NJ, USA) at 37℃ for 60 min. Cells were cultured in α-MEM (Thermo Fisher Scientific, Carlsbad, CA, USA) supplemented with 20% fetal bovine serum (FBS), 100 unit/ml penicillin, and 0.1 mg/ml streptomycin at 37℃ in a humidified incubator with 5% CO_2 and 1% O_2 to prevent damage by oxygen and to maintain the viability of *Sod1*$^{-/-}$ fibroblasts. During the subsequent experiments, the cells were cultured to investigate cellular phenotypes under a general condition (20% O_2). The fibroblasts were cultured in 12-well culture plates (Falcon BD, Franklin Lakes, NJ, USA) with or without 50 μM SYR for 72 h and then incubated with 10 μM CM-H_2DCFDA (DCF, Thermo Fisher Scientific, Carlsbad, CA, USA) for 30 min at 37℃. After incubation, cells were trypsinized and resuspended in PBS(-). Fluorescence intensity was assessed using a flow cytometer (BD FACSCanto II, BD Biosciences, Franklin Lakes, NJ, USA).

Outgrowth assay

Adult *Sod1*$^{+/+}$ and *Sod1*$^{-/-}$ mouse back skin was sterilized with 70% ethanol, rinsed with PBS (Takara Bio Inc., Shiga, Japan) and punched out into discs measuring 5 mm in diameter using a dermal punch (Nipro, Tokyo, Japan) [19]. The punched skin discs were placed into a 24-well culture plate (Falcon BD, Franklin Lakes, NJ, USA) and cultured with or without 50 μM SYR in α-MEM containing 20% FBS, 100 units/mL penicillin, and 0.1 mg/ml streptomycin at 37℃ in a humidified incubator with 5% CO_2 and 20% O_2. The number of outgrowing fibroblasts that originated from the mouse skin discs was directly counted at 96 h after culture.

Statistical analysis

Statistical analyses were performed using Student's *t*-test for comparisons between two groups and one-way analysis of variance (ANOVA) with Dunnett's multiple comparisons test for comparisons among three groups when comparing dose responses. Differences were considered significant when the P values were less than 0.05. All data are expressed as the mean ± standard deviation (SD).

References

1 Nakae, J. *et al.* Regulation of insulin action and pancreatic beta-cell function by mutated alleles of the gene encoding forkhead transcription factor Foxo1. *Nature genetics* **32**, 245-253, doi:10.1038/ng890 (2002).

2 Bluher, M., Kahn, B. B. & Kahn, C. R. Extended longevity in mice lacking the insulin receptor in adipose tissue. *Science (New York, N.Y.)* **299**, 572-574, doi:10.1126/science.1078223 (2003).

3 Holzenberger, M. *et al.* IGF-1 receptor regulates lifespan and resistance to oxidative stress in mice. *Nature* **421**, 182-187, doi:10.1038/nature01298 (2003).

4 Hu, M. C. *et al.* IkappaB kinase promotes tumorigenesis through inhibition of forkhead FOXO3a. *Cell* **117**, 225-237 (2004).

5 Paik, J. H. *et al.* FoxOs are lineage-restricted redundant tumor suppressors and regulate endothelial cell homeostasis. *Cell* **128**, 309-323, doi:10.1016/j.cell.2006.12.029 (2007).

6 Biggs, W. H., 3rd, Cavenee, W. K. & Arden, K. C. Identification and characterization of members of the FKHR (FOX O) subclass of winged-helix transcription factors in the mouse. *Mammalian genome : official journal of the International Mammalian Genome Society* **12**, 416-425, doi:10.1007/s003350020002 (2001).

7 Jacobs, F. M. *et al.* FoxO6, a novel member of the FoxO class of transcription factors with distinct shuttling dynamics. *The Journal of biological chemistry* **278**, 35959-35967, doi:10.1074/jbc.M302804200 (2003).

8 van der Vos, K. E. & Coffer, P. J. The extending network of FOXO transcriptional target genes. *Antioxidants & redox signaling* **14**, 579-592, doi:10.1089/ars.2010.3419 (2011).

9 Hosaka, T. *et al.* Disruption of forkhead transcription factor (FOXO) family members in

mice reveals their functional diversification. *Proceedings of the National Academy of Sciences of the United States of America* **101**, 2975-2980, doi:10.1073/pnas.0400093101 (2004).

10 Castrillon, D. H., Miao, L., Kollipara, R., Horner, J. W. & DePinho, R. A. Suppression of ovarian follicle activation in mice by the transcription factor Foxo3a. *Science (New York, N.Y.)* **301**, 215-218, doi:10.1126/science.1086336 (2003).

11 Durgan, J. *et al.* SOS1 and Ras regulate epithelial tight junction formation in the human airway through EMP1. *EMBO reports* **16**, 87-96, doi:10.15252/embr.201439218 (2015).

12 Van Der Heide, L. P., Hoekman, M. F. & Smidt, M. P. The ins and outs of FoxO shuttling: mechanisms of FoxO translocation and transcriptional regulation. *The Biochemical journal* **380**, 297-309, doi:10.1042/bj20040167 (2004).

13 Obsil, T. & Obsilova, V. Structure/function relationships underlying regulation of FOXO transcription factors. *Oncogene* **27**, 2263-2275, doi:10.1038/onc.2008.20 (2008).

14 Partridge, L. & Bruning, J. C. Forkhead transcription factors and ageing. *Oncogene* **27**, 2351-2363, doi:10.1038/onc.2008.28 (2008).

15 Heffetz, D., Rutter, W. J. & Zick, Y. The insulinomimetic agents H2O2 and vanadate stimulate tyrosine phosphorylation of potential target proteins for the insulin receptor kinase in intact cells. *The Biochemical journal* **288 (Pt 2)**, 631-635 (1992).

16 Bi, W. *et al.* c-Jun N-terminal kinase enhances MST1-mediated pro-apoptotic signaling through phosphorylation at serine 82. *The Journal of biological chemistry* **285**, 6259-6264, doi:10.1074/jbc.M109.038570 (2010).

17 Essers, M. A. *et al.* FOXO transcription factor activation by oxidative stress mediated by the small GTPase Ral and JNK. *The EMBO journal* **23**, 4802-4812,

doi:10.1038/sj.emboj.7600476 (2004).

18 Ueda, S. *et al.* Redox control of cell death. *Antioxidants & redox signaling* **4**, 405-414, doi:10.1089/15230860260196209 (2002).

19 Watanabe, K. *et al.* Superoxide dismutase 1 loss disturbs intracellular redox signaling, resulting in global age-related pathological changes. *BioMed research international* **2014**, 140165, doi:10.1155/2014/140165 (2014).

20 Imamura, Y. *et al.* Drusen, choroidal neovascularization, and retinal pigment epithelium dysfunction in SOD1-deficient mice: a model of age-related macular degeneration. *Proceedings of the National Academy of Sciences of the United States of America* **103**, 11282-11287, doi:10.1073/pnas.0602131103 (2006).

21 Uchiyama, S., Shimizu, T. & Shirasawa, T. CuZn-SOD deficiency causes ApoB degradation and induces hepatic lipid accumulation by impaired lipoprotein secretion in mice. *The Journal of biological chemistry* **281**, 31713-31719, doi:10.1074/jbc.M603422200 (2006).

22 Kondo, Y. *et al.* Senescence marker protein-30/superoxide dismutase 1 double knockout mice exhibit increased oxidative stress and hepatic steatosis. *FEBS open bio* **4**, 522-532, doi:10.1016/j.fob.2014.05.003 (2014).

23 Murakami, K. *et al.* Skin atrophy in cytoplasmic SOD-deficient mice and its complete recovery using a vitamin C derivative. *Biochemical and biophysical research communications* **382**, 457-461, doi:10.1016/j.bbrc.2009.03.053 (2009).

24 Shibuya, S. *et al.* Collagen peptide and vitamin C additively attenuate age-related skin atrophy in Sod1-deficient mice. *Bioscience, biotechnology, and biochemistry* **78**, 1212-1220, doi:10.1080/09168451.2014.915728 (2014).

25 Nojiri, H. *et al.* Cytoplasmic superoxide causes bone fragility owing to low-turnover osteoporosis and impaired collagen cross-linking. *Journal of bone and mineral research : the official journal of the American Society for Bone and Mineral Research* **26**, 2682-2694, doi:10.1002/jbmr.489 (2011).

26 Morikawa, D. *et al.* Cytoplasmic reactive oxygen species and SOD1 regulate bone mass during mechanical unloading. *Journal of bone and mineral research : the official journal of the American Society for Bone and Mineral Research* **28**, 2368-2380, doi:10.1002/jbmr.1981 (2013).

27 Murakami, K. & Shimizu, T. Cytoplasmic superoxide radical: a possible contributing factor to intracellular Abeta oligomerization in Alzheimer disease. *Communicative & integrative biology* **5**, 255-258, doi:10.4161/cib.19548 (2012).

28 Noda, Y., Ota, K., Shirasawa, T. & Shimizu, T. Copper/zinc superoxide dismutase insufficiency impairs progesterone secretion and fertility in female mice. *Biology of reproduction* **86**, 1-8, doi:10.1095/biolreprod.111.092999 (2012).

29 Kojima, T. *et al.* Age-related dysfunction of the lacrimal gland and oxidative stress: evidence from the Cu,Zn-superoxide dismutase-1 (Sod1) knockout mice. *The American journal of pathology* **180**, 1879-1896, doi:10.1016/j.ajpath.2012.01.019 (2012).

30 Ibrahim, O. M. *et al.* Oxidative stress induced age dependent meibomian gland dysfunction in Cu, Zn-superoxide dismutase-1 (Sod1) knockout mice. *PloS one* **9**, e99328, doi:10.1371/journal.pone.0099328 (2014).

31 Morikawa, D. *et al.* Contribution of oxidative stress to the degeneration of rotator cuff entheses. *Journal of shoulder and elbow surgery* **23**, 628-635, doi:10.1016/j.jse.2014.01.041 (2014).

32 Shibuya, S. *et al.* Palladium and platinum nanoparticles attenuate aging-like skin atrophy via antioxidant activity in mice. *PloS one* **9**, e109288, doi:10.1371/journal.pone.0109288 (2014).

33 Lerner, A. B. & Fitzpatrick, T. B. Biochemistry of melanin formation. *Physiological reviews* **30**, 91-126, doi:10.1152/physrev.1950.30.1.91 (1950).

34 Picardo, M. *et al.* Correlation between antioxidants and phototypes in melanocytes cultures. A possible link of physiologic and pathologic relevance. *The Journal of investigative dermatology* **113**, 424-425, doi:10.1046/j.1523-1747.1999.00714.x (1999).

35 Cho, S. Y., Cho, M., Seo, D. B., Lee, S. J. & Suh, Y. Identification of a small molecule activator of SIRT1 gene expression. *Aging* **5**, 174-182, doi:10.18632/aging.100539 (2013).

36 Ho, K. K., Myatt, S. S. & Lam, E. W. Many forks in the path: cycling with FoxO. *Oncogene* **27**, 2300-2311, doi:10.1038/onc.2008.23 (2008).

37 Kampkotter, A. *et al.* Effects of the flavonoids kaempferol and fisetin on thermotolerance, oxidative stress and FoxO transcription factor DAF-16 in the model organism Caenorhabditis elegans. *Archives of toxicology* **81**, 849-858, doi:10.1007/s00204-007-0215-4 (2007).

38 Yao, R. & Cooper, G. M. Requirement for phosphatidylinositol-3 kinase in the prevention of apoptosis by nerve growth factor. *Science (New York, N.Y.)* **267**, 2003-2006 (1995).

39 Burgering, B. M. & Kops, G. J. Cell cycle and death control: long live Forkheads. *Trends in biochemical sciences* **27**, 352-360 (2002).

40 Brunet, A. *et al.* Akt promotes cell survival by phosphorylating and inhibiting a Forkhead transcription factor. *Cell* **96**, 857-868 (1999).

41 Kops, G. J. *et al.* Control of cell cycle exit and entry by protein kinase B-regulated forkhead transcription factors. *Molecular and cellular biology* **22**, 2025-2036 (2002).

42 Brownawell, A. M., Kops, G. J., Macara, I. G. & Burgering, B. M. Inhibition of nuclear import by protein kinase B (Akt) regulates the subcellular distribution and activity of the forkhead transcription factor AFX. *Molecular and cellular biology* **21**, 3534-3546, doi:10.1128/mcb.21.10.3534-3546.2001 (2001).

43 Fujiwara, Y. *et al.* Effect of simultaneous administration of vitamin C, L-cysteine and vitamin E on the melanogenesis. *BioFactors (Oxford, England)* **21**, 415-418 (2004).

44 Hu, Z. M., Zhou, Q., Lei, T. C., Ding, S. F. & Xu, S. Z. Effects of hydroquinone and its glucoside derivatives on melanogenesis and antioxidation: Biosafety as skin whitening agents. *Journal of dermatological science* **55**, 179-184, doi:10.1016/j.jdermsci.2009.06.003 (2009).

45 Kim, C. K. *et al.* Ginseng Berry Extract Prevents Atherogenesis via Anti-Inflammatory Action by Upregulating Phase II Gene Expression. *Evidence-based complementary and alternative medicine : eCAM* **2012**, 490301, doi:10.1155/2012/490301 (2012).

46 Kim, J. *et al.* Effects of Korean ginseng berry on skin antipigmentation and antiaging via FoxO3a activation. *Journal of ginseng research* **41**, 277-283, doi:10.1016/j.jgr.2016.05.005 (2017).

47 Kim, J., Ishihara, N. & Lee, T. R. A DAF-16/FoxO3a-dependent longevity signal is initiated by antioxidants. *BioFactors (Oxford, England)* **40**, 247-257, doi:10.1002/biof.1146 (2014).

48 Wang, C. *et al.* Apelin induces vascular smooth muscle cells migration via a PI3K/Akt/FoxO3a/MMP-2 pathway. *The international journal of biochemistry & cell*

biology **69**, 173-182, doi:10.1016/j.biocel.2015.10.015 (2015).

49 Cornelius, C., Perrotta, R., Graziano, A., Calabrese, E. J. & Calabrese, V. Stress responses, vitagenes and hormesis as critical determinants in aging and longevity: Mitochondria as a "chi". *Immunity & ageing : I & A* **10**, 15, doi:10.1186/1742-4933-10-15 (2013).

50 de Keizer, P. L., Burgering, B. M. & Dansen, T. B. Forkhead box o as a sensor, mediator, and regulator of redox signaling. *Antioxidants & redox signaling* **14**, 1093-1106, doi:10.1089/ars.2010.3403 (2011).

51 Putker, M. *et al.* Redox-dependent control of FOXO/DAF-16 by transportin-1. *Molecular cell* **49**, 730-742, doi:10.1016/j.molcel.2012.12.014 (2013).

52 van der Vos, K. E. & Coffer, P. J. FOXO-binding partners: it takes two to tango. *Oncogene* **27**, 2289-2299, doi:10.1038/onc.2008.22 (2008).

53 Hu, P., Geles, K. G., Paik, J. H., DePinho, R. A. & Tjian, R. Codependent activators direct myoblast-specific MyoD transcription. *Developmental cell* **15**, 534-546, doi:10.1016/j.devcel.2008.08.018 (2008).

54 Shoag, J. *et al.* PGC-1 coactivators regulate MITF and the tanning response. *Molecular cell* **49**, 145-157, doi:10.1016/j.molcel.2012.10.027 (2013).

55 Corton, J. C. & Brown-Borg, H. M. Peroxisome proliferator-activated receptor gamma coactivator 1 in caloric restriction and other models of longevity. *The journals of gerontology. Series A, Biological sciences and medical sciences* **60**, 1494-1509 (2005).

56 Jung, H., Bae, J., Ko, S. K. & Sohn, U. D. Ultrasonication processed Panax ginseng berry extract induces apoptosis through an intrinsic apoptosis pathway in HepG2 cells. *Archives of pharmacal research* **39**, 855-862, doi:10.1007/s12272-016-0760-6 (2016).

57 Zhang, W. *et al.* Ginseng Berry Extract Attenuates Dextran Sodium Sulfate-Induced

Acute and Chronic Colitis. *Nutrients* **8**, 199, doi:10.3390/nu8040199 (2016).

58 Kim, M. H. *et al.* The involvement of ginseng berry extract in blood flow via regulation of blood coagulation in rats fed a high-fat diet. *Journal of ginseng research* **41**, 120-126, doi:10.1016/j.jgr.2016.01.004 (2017).

59 Jimenez, Z. *et al.* Assessment of radical scavenging, whitening and moisture retention activities of Panax ginseng berry mediated gold nanoparticles as safe and efficient novel cosmetic material. *Artificial cells, nanomedicine, and biotechnology* **46**, 333-340, doi:10.1080/21691401.2017.1307216 (2018).

60 Wolkow, C. A., Kimura, K. D., Lee, M. S. & Ruvkun, G. Regulation of C. elegans life-span by insulinlike signaling in the nervous system. *Science (New York, N.Y.)* **290**, 147-150 (2000).

61 Libina, N., Berman, J. R. & Kenyon, C. Tissue-specific activities of C. elegans DAF-16 in the regulation of lifespan. *Cell* **115**, 489-502 (2003).

62 Kyoung Kim, H. *et al.* Down-regulation of a forkhead transcription factor, FOXO3a, accelerates cellular senescence in human dermal fibroblasts. *The journals of gerontology. Series A, Biological sciences and medical sciences* **60**, 4-9 (2005).

63 Mandinova, A. *et al.* The FoxO3a gene is a key negative target of canonical Notch signalling in the keratinocyte UVB response. *The EMBO journal* **27**, 1243-1254, doi:10.1038/emboj.2008.45 (2008).

64 Wang, X., Chen, W. R. & Xing, D. A pathway from JNK through decreased ERK and Akt activities for FOXO3a nuclear translocation in response to UV irradiation. *Journal of cellular physiology* **227**, 1168-1178, doi:10.1002/jcp.22839 (2012).

65 Im, J., Hergert, P. & Nho, R. S. Reduced FoxO3a expression causes low autophagy in

idiopathic pulmonary fibrosis fibroblasts on collagen matrices. *American journal of physiology. Lung cellular and molecular physiology* **309**, L552-561, doi:10.1152/ajplung.00079.2015 (2015).

66 Nho, R. S., Hergert, P., Kahm, J., Jessurun, J. & Henke, C. Pathological alteration of FoxO3a activity promotes idiopathic pulmonary fibrosis fibroblast proliferation on type i collagen matrix. *The American journal of pathology* **179**, 2420-2430, doi:10.1016/j.ajpath.2011.07.020 (2011).

67 Cho, S. *et al.* Syringaresinol protects against hypoxia/reoxygenation-induced cardiomyocytes injury and death by destabilization of HIF-1alpha in a FOXO3-dependent mechanism. *Oncotarget* **6**, 43-55, doi:10.18632/oncotarget.2723 (2015).

68 Schmittgen, T. D. & Livak, K. J. Analyzing real-time PCR data by the comparative C(T) method. *Nature protocols* **3**, 1101-1108 (2008).

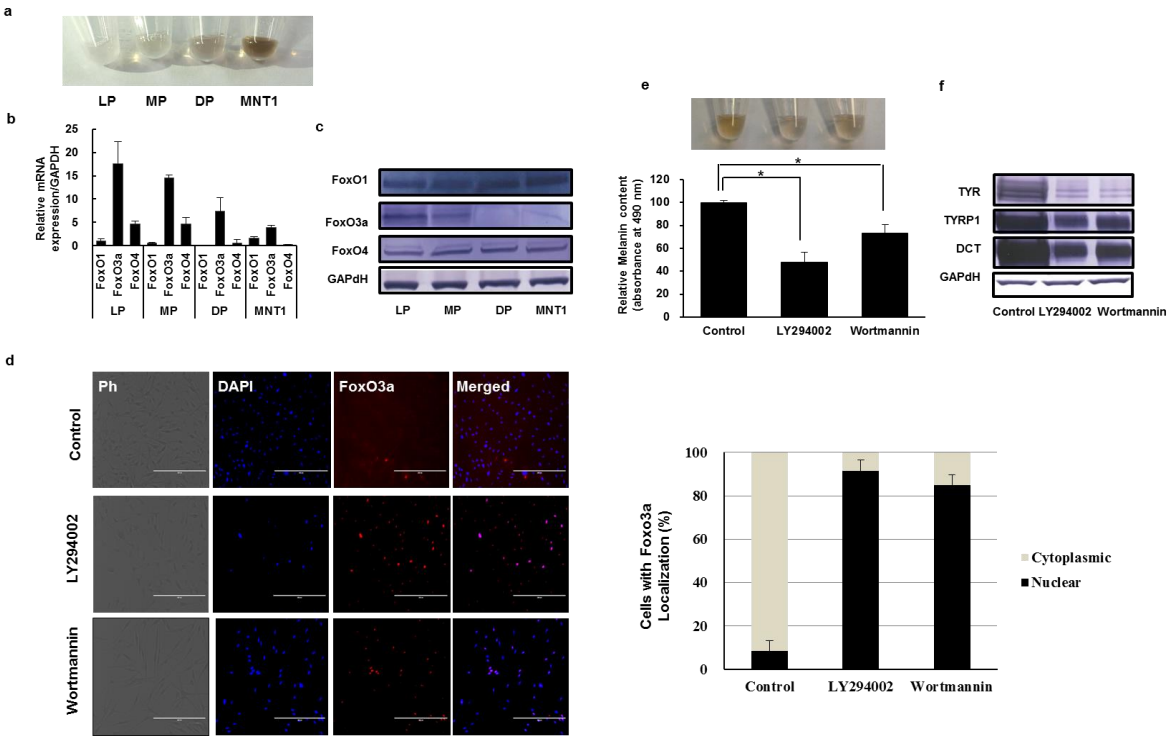

Figure 1. The FoxO proteins expression level and the melanogenesis regulation by FoxO3a in primary melanocytes. (**a**) The melanin levels were visualized after dissolving cell pellets with 1 N NaOH in lightly pigmented (LP), moderately pigmented [37], and darkly pigmented (DP) melanocytes and MNT1 cells. (**b**) The FoxO1, FoxO3a, and FoxO4 mRNA expression levels of in the LP, MP, and DP melanocytes and MNT1 cells. The data represent mean ± S.D. from three independent experiments. (**c**) The FoxO proteins expression levels in pigmented cells were determined by western blot analysis. (**d**) PI3K inhibitors LY294002 (500 μM) or wortmannin (1 μM) treated in primary melanocytes for 48 h. The cells were stained with an anti-FoxO3a antibody (FoxO3a; red) and DAPI (nucleus; blue). Cell with FoxO3a localization were counted and depicted by EVOSfl digital fluorescence microscope. Representative images are shown. Control, vehicle alone-treated; Ph, phase-contrast image. Scale bars, 200 μm. (**e**) Melanin levels were visualized under PI3K inhibitors LY294002 (500 μM) and wortmannin (1 μM) treatment in primary melanocytes for 5 days. The quantitative melanin levels were determined by a spectrophotometer with absorbance at 490 nm. (**f**) LY294002 (500 μM) or wortmannin (1 μM) treated in primary melanocytes for 48 h, and then the cell lysates were analyzed by western blotting analysis. Control: vehicle alone-treated.

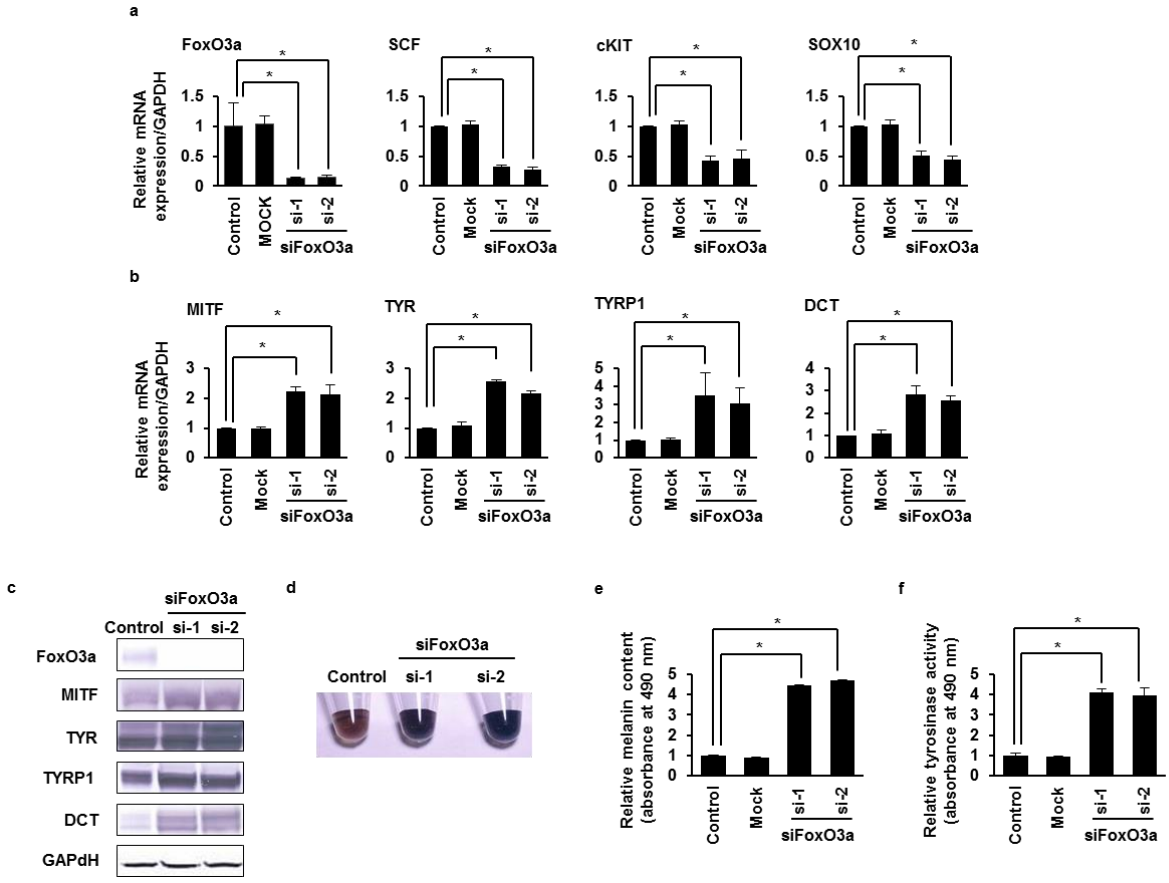

Figure 2. Melanogenesis regulation by FoxO3a is induced by melanogenic genes modulation. FoxO3a siRNAs were transfected in MNT1 cells for 48 h. Down-regulated (**a**) or up-regulated (**b**) genes were estimated via RT-qPCR. *$p < 0.05$. (**c**) The cell lysates were analyzed via western blot after FoxO3a siRNAs treatment. The melanin levels (**d, e**) and tyrosinase activity (**f**) were measured using a spectrophotometer at 490 nm. Control: untreated; Mock: control siRNA; si-1, 2: siRNA against FoxO3a. The values of three independent experiments are presented (mean ± S.D.). *$p < 0.05$.

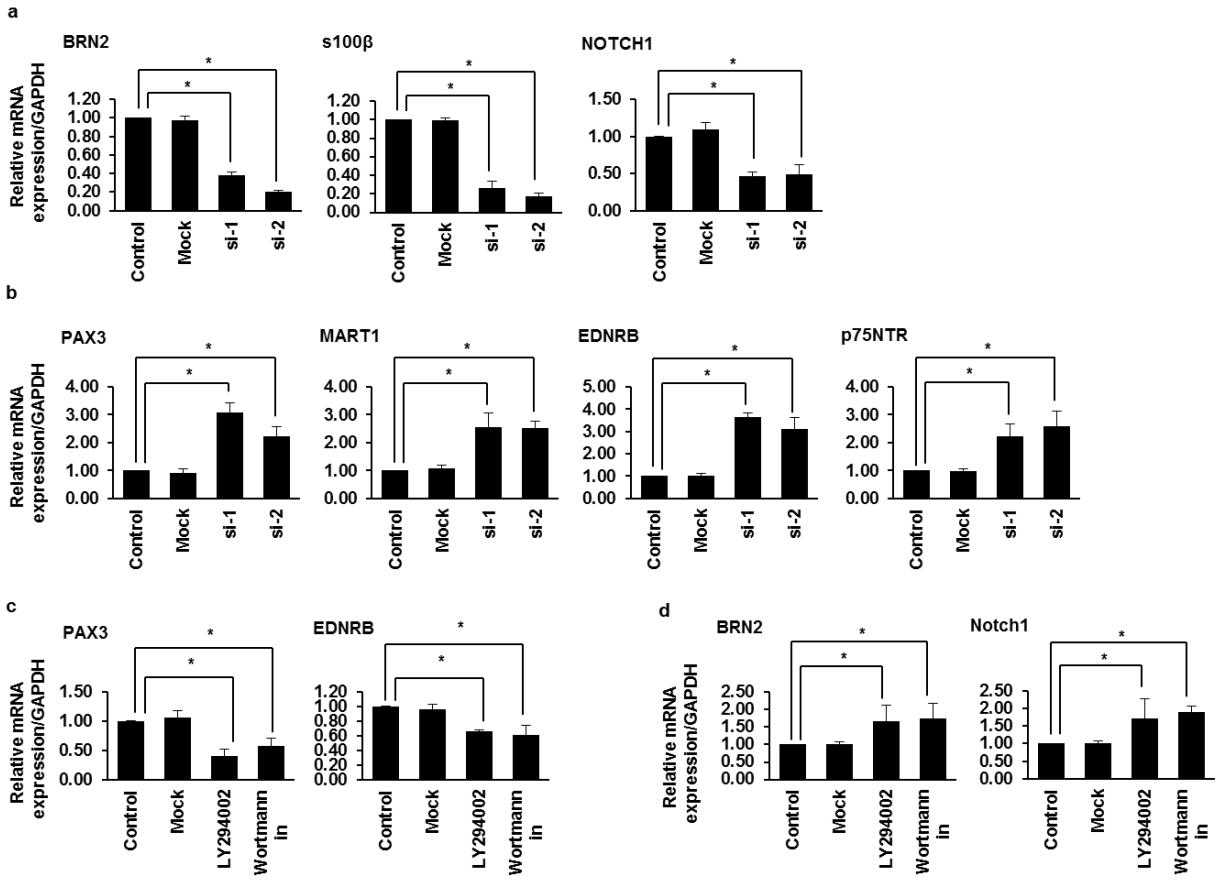

Figure 3. The regulation of FoxO3a expression affects melanogenesis-related genes. Down-regulated (**a**) or up-regulated (**b**) genes following FoxO3a siRNA treatment (si-1 or -2) are shown. *$p < 0.05$. Down-regulated (**c**) or up-regulated (**d**) genes after treatment with the PI3K inhibitors LY294002 and wortmannin are displayed. *$p < 0.05$.

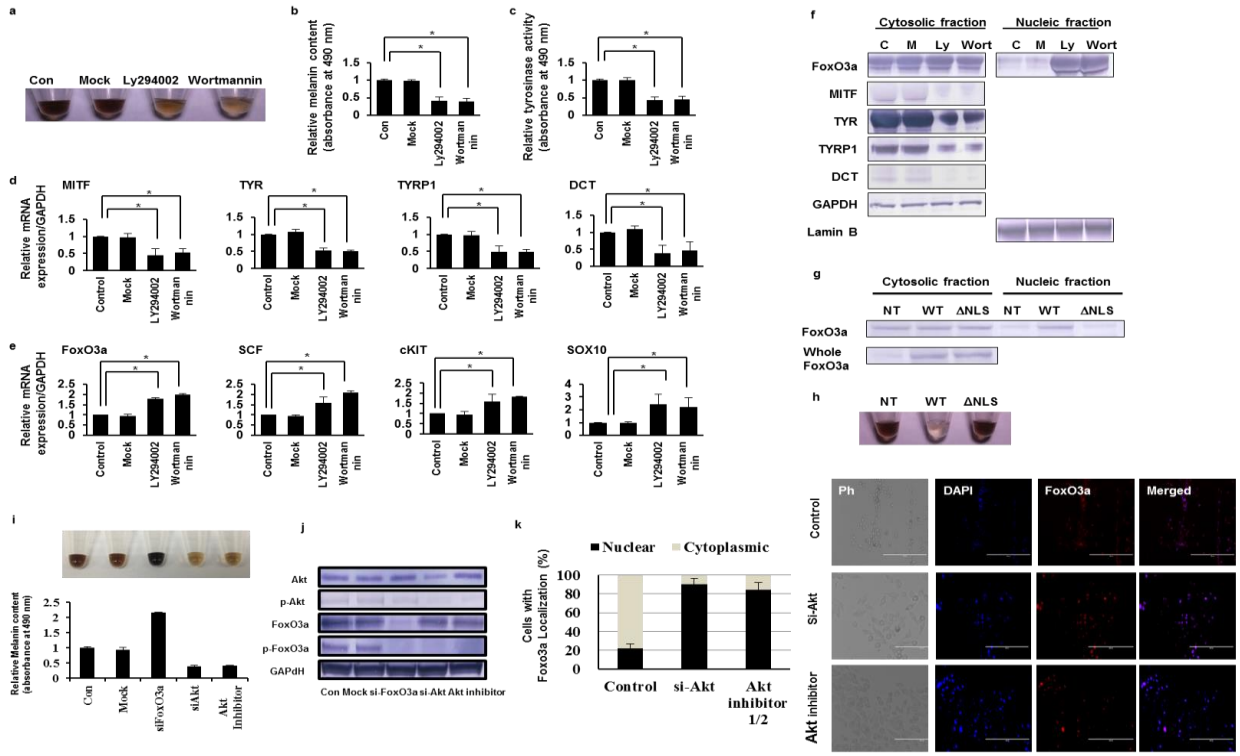

Figure 4. FoxO3a regulates melanogenesis by its nuclear translocation. (**a**) The melanin levels visualized in MNT1 cells under treatment with the PI3K inhibitors LY294002 (500 μM) and wortmannin (1 μM) for 48 h. The quantitative melanin levels (**b**) and tyrosinase activity (**c**) were measured by a spectrophotometer at 490 nm. The down-regulated (**d**) and up-regulated (**e**) genes are shown via RT-qPCR after the treatment with the PI3K inhibitors. *$p < 0.05$. The data are presented from three independent experiments (mean ± S.D.). (**f**) The proteins, including FoxO3a, were analyzed via western blot analysis in cytosolic and nuclear cell fractionation after PI3K inhibitor treatment. Lamin B was used as a marker of the nuclear fraction. C, untreated; M, vehicle alone-treated; Ly, LY294002; Wort, wortmannin. (**g**) The wild-type FoxO3a (WT) or mutants FoxO3a with a deleted nuclear localization signal (ΔNLS) constructs were designed and transfected into MNT1 cells. FoxO3a protein expression was analyzed by western blot in cytosolic and nuclear portions of total protein. NT, non-treated; WT, wild-type; ΔNLS, nuclear localization signal deleted mutant. (**h**) The MNT1 cells were transfected with overexpression of the wild-type or mutant FoxO3a, then melanin were visualized. The siRNAs against FoxO3a or Akt was treated in MNT1 cells; 10 μM Akt inhibitor was treated for 48 h. The melanin levels (**i**), and the protein levels (**j**) of each protein were analyzed. Con: vehicle alone-treated; Mock: control siRNA. (**k**) MNT1 cells were transfected with FoxO3a or Akt siRNAs; the treatment of 10 μM Akt inhibitor was performed for 48 h. The cells were stained with an anti-FoxO3a antibody (FoxO3a; red) and DAPI (nucleus; blue). The representative images were acquired using fluorescence microscopy. Ph, phase-contrast image. Scale bars, 200 μm. Cell with FoxO3a localization were counted and depicted by EVOSfl digital fluorescence microscope.

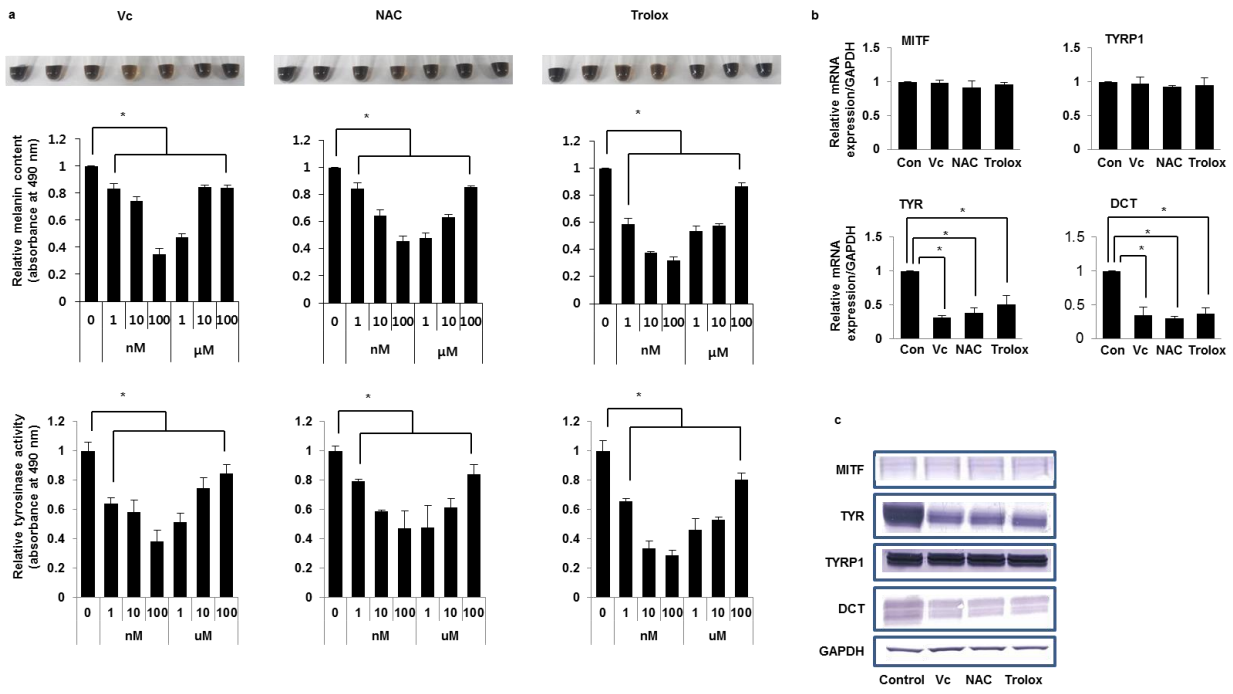

Figure 5. Antioxidants reduce melanogenesis and especially inhibit tyrosinase and DCT. (**a**) The melanin levels (upper panel) and tyrosinase activity (lower panel) is shown after the treatment with each antioxidant at various concentrations for 48 h. The melanogenesis–related genes expression levels, mRNA (**b**) and protein (**c**) were analyzed via RT-qPCR after the treatment with each antioxidant (100 nM) for 48 h. *$p < 0.05$. Con: vehicle only; Vc: vitamin C; NAC: N-acetyl cysteine. The data are represented by three independent experiments (mean ± S.D.).

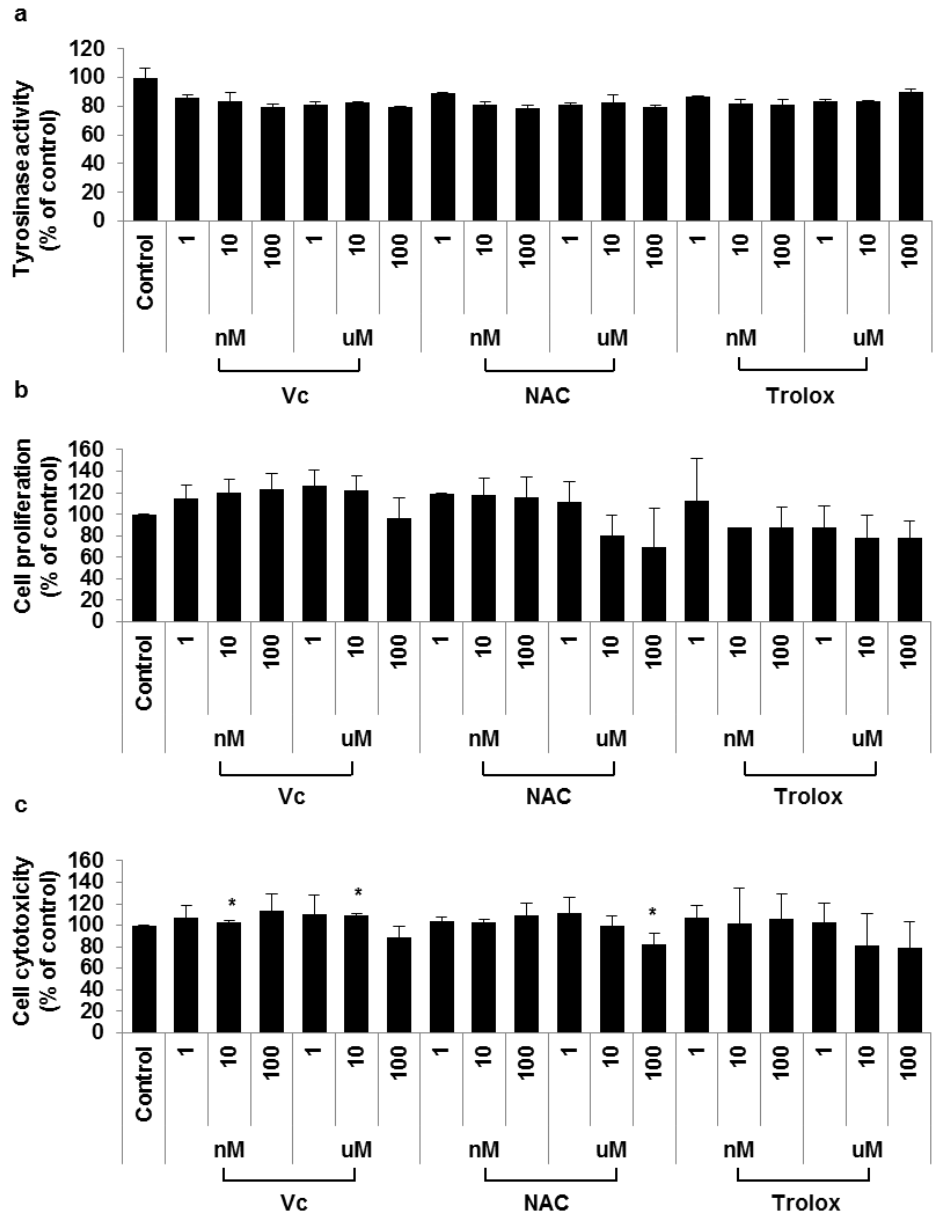

Figure 6. The effects of antioxidants on tyrosinase activity, cell proliferation, and cell cytotoxicity. (**a**) Mushroom tyrosinase was treated with 1 nM – 100 μM of each antioxidant *in vitro*. Cell proliferation (**b**) and cytotoxicity (**c**) were analyzed by cell quantification and MTT assay, respectively, after treatment with each antioxidant. Vc, Vitamin C; NAC, N-Acetylcysteine.

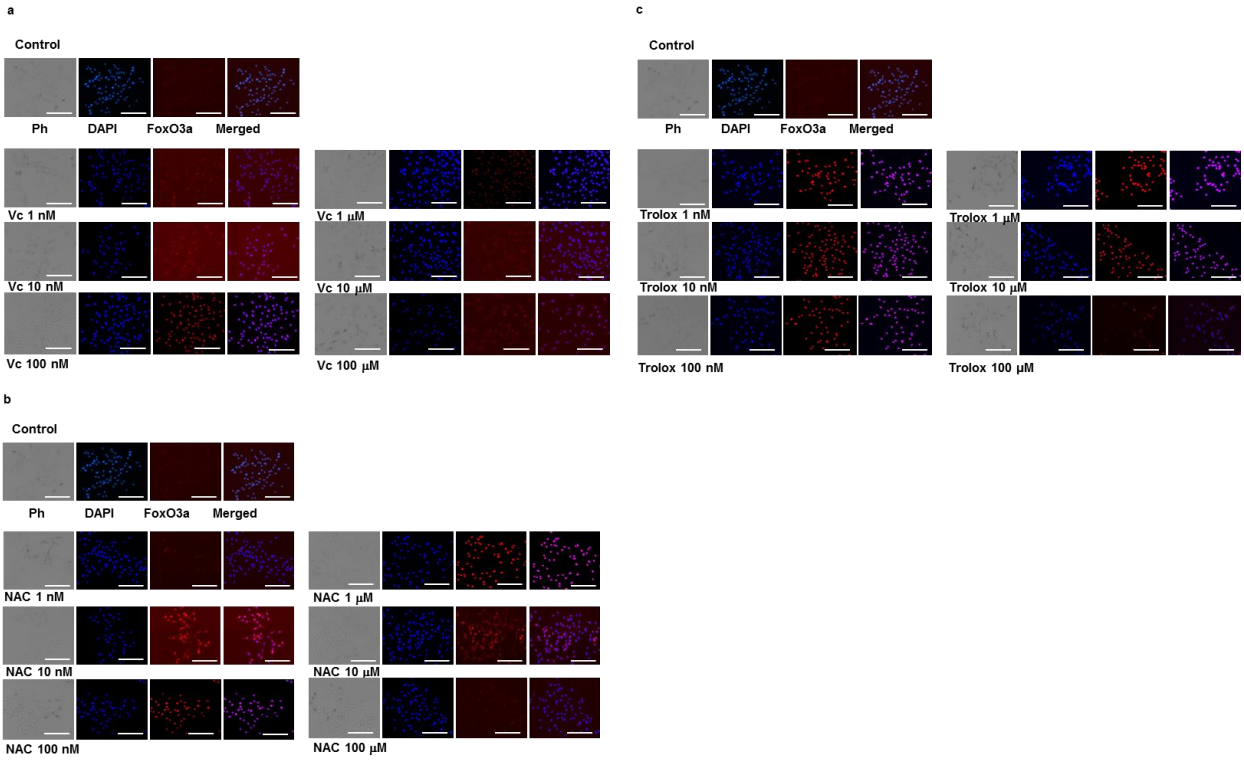

Figure 7. The nuclear translocation of FoxO3a is dependent on antioxidant concentrations. Nuclear translocation of FoxO3a after treatment with various concentrations of Vc (**a**), NAC (**b**), or Trolox (**c**) was detected via immunofluorescence using an anti-FoxO3a antibody. Ph, phase-contrast image; DAPI, blue; FoxO3a, red; and merged images are presented. Scale bars, 100 μm.

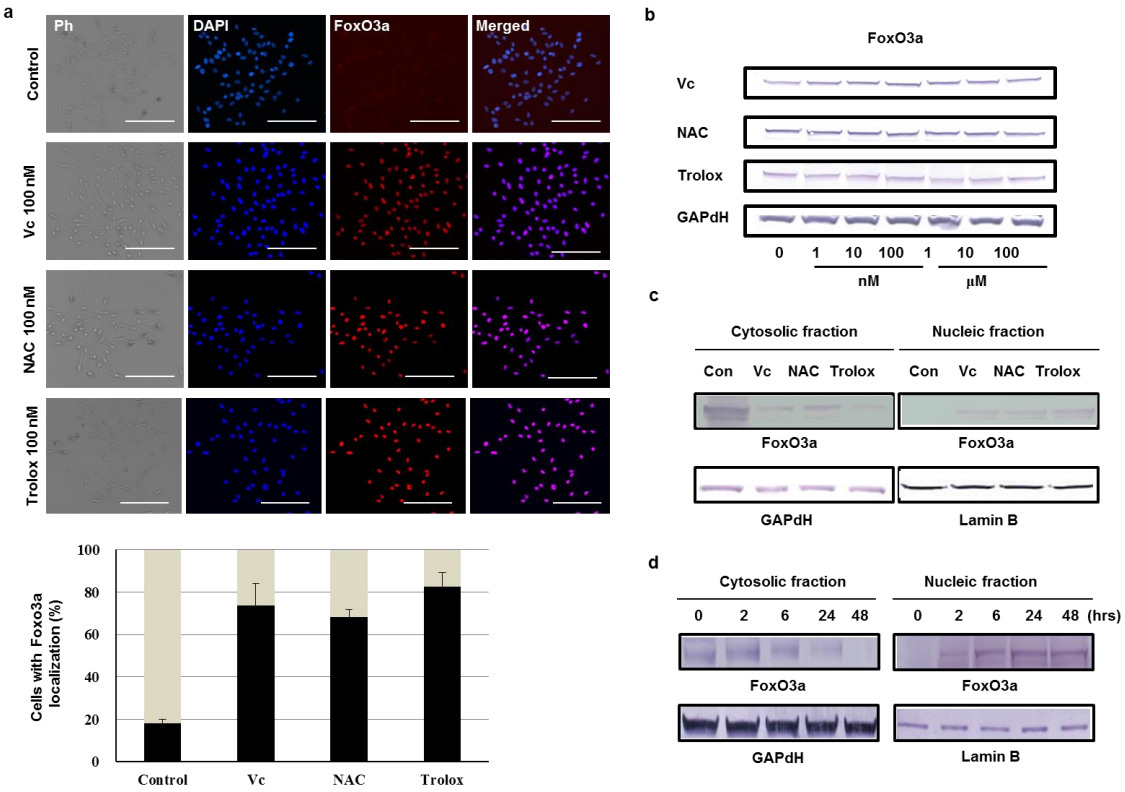

Figure 8. FoxO3a nuclear translocation is induced by antioxidants treatment. (**a**) The cells were stained with an anti-FoxO3a antibody (FoxO3a; red) and DAPI (nucleus; blue) after antioxidants (100 nM) treatment for 48 h. The representative images were acquired by fluorescence microscopy. Ph, phase-contrast image. Scale bars, 100 μm. Cell with FoxO3a localization were counted and depicted by EVOSfl digital fluorescence microscope. (**b**) After the treatment with each antioxidant, total FoxO3a protein was analyzed by western blot. (**c**) FoxO3a was examined via western blot in cytosolic and nuclear fractions of MNT1 cells under treatment with 100 nM of each antioxidant for 48 h. (**d**) 100 nM of vitamin C was treated in MNT1 cells for 2, 6, 24, or 48 h and then cellular fractionation was performed. FoxO3a was detected in cytosolic and nuclear fractions by western blot. Con: vehicle only; Vc: vitamin C; NAC: N-acetyl cysteine. GAPDH or lamin B was used as a marker of the cytosolic fraction or nuclear fraction, respectively.

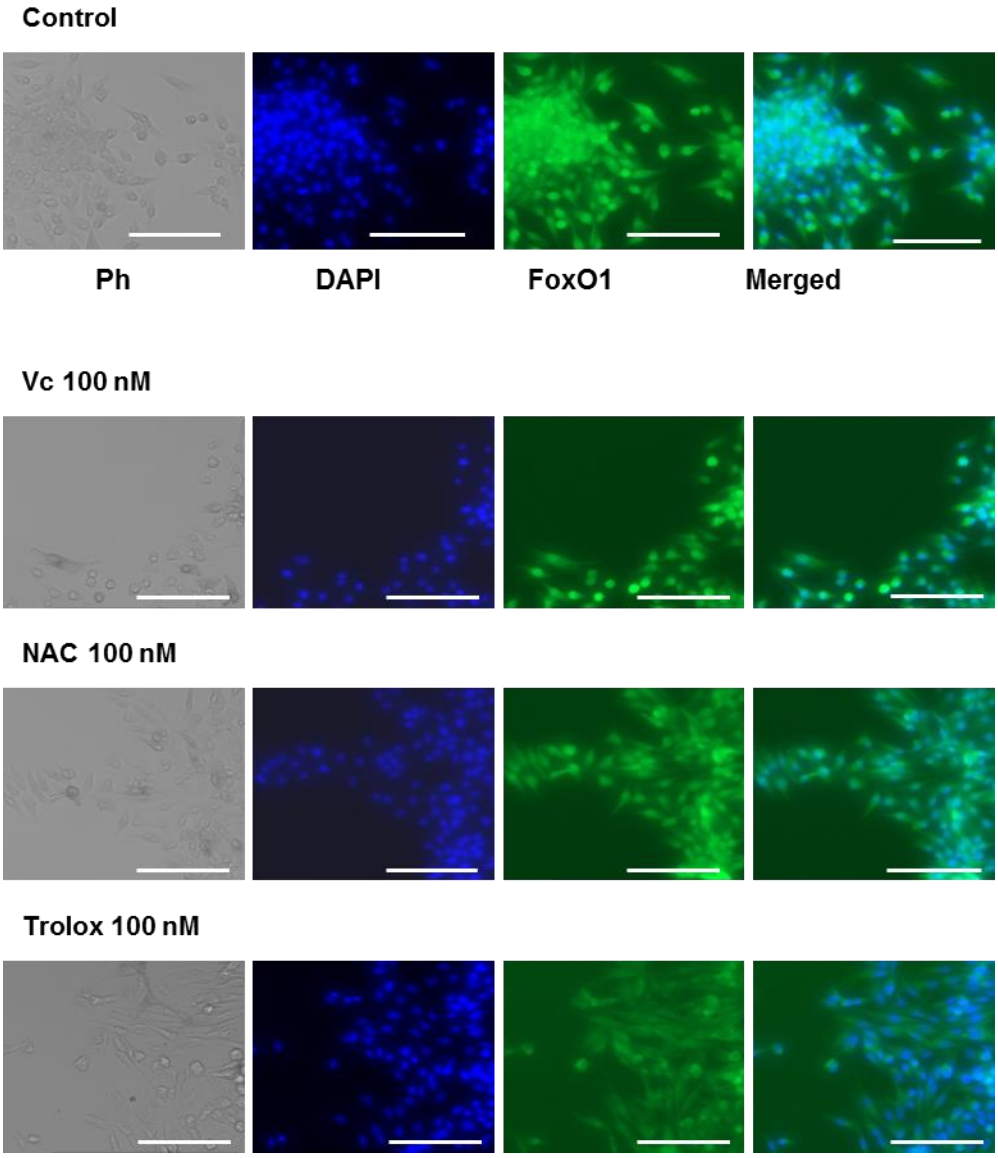

Figure 9. FoxO1 nuclear translocation was not affected by antioxidant treatment. The nuclear translocation of FoxO1 after treatment with each antioxidant (100 nM) was examined via immunofluorescence using an anti-FoxO1 antibody. Ph, phase-contrast image; DAPI, blue; FoxO3a, green; and merged images are presented. Scale bars, 100 μm.

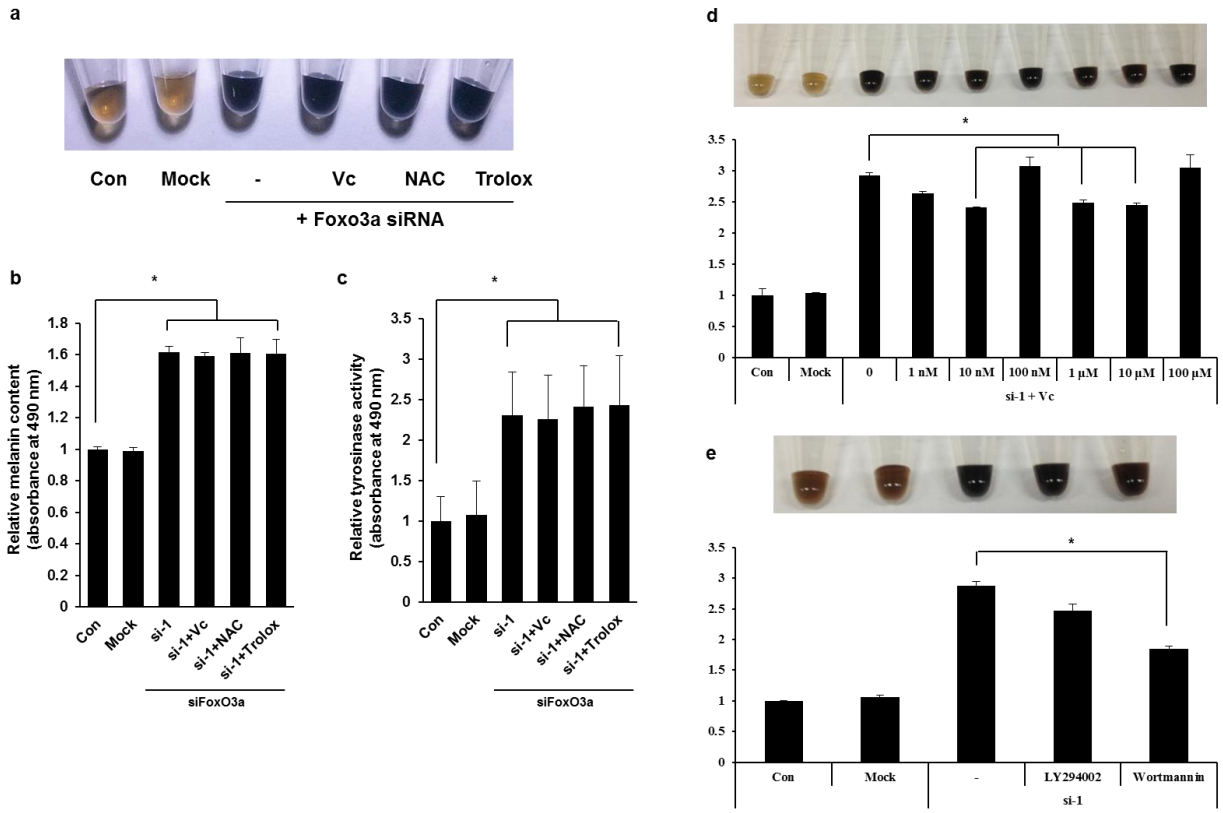

Figure 10. Regulation of melanin synthesis by antioxidant and PI3K mediates FoxO3a. (**a-c**) 100 nM of each antioxidant and a 0-100 μM dose range of vitamin C (**d**), or PI3K inhibitors (**e**) was treated in MNT1 cells after FoxO3a siRNAs were applied. The melanin levels (**a, b, d, and e**) and the tyrosinase activity (**c**) was determined. Con: vehicle alone; Mock: control siRNA; si: siRNA against FoxO3a; Vc: vitamin C; NAC: N-acetyl cysteine. The data are shown as the mean ± S.D. of three independent experiments. *$p < 0.05$.

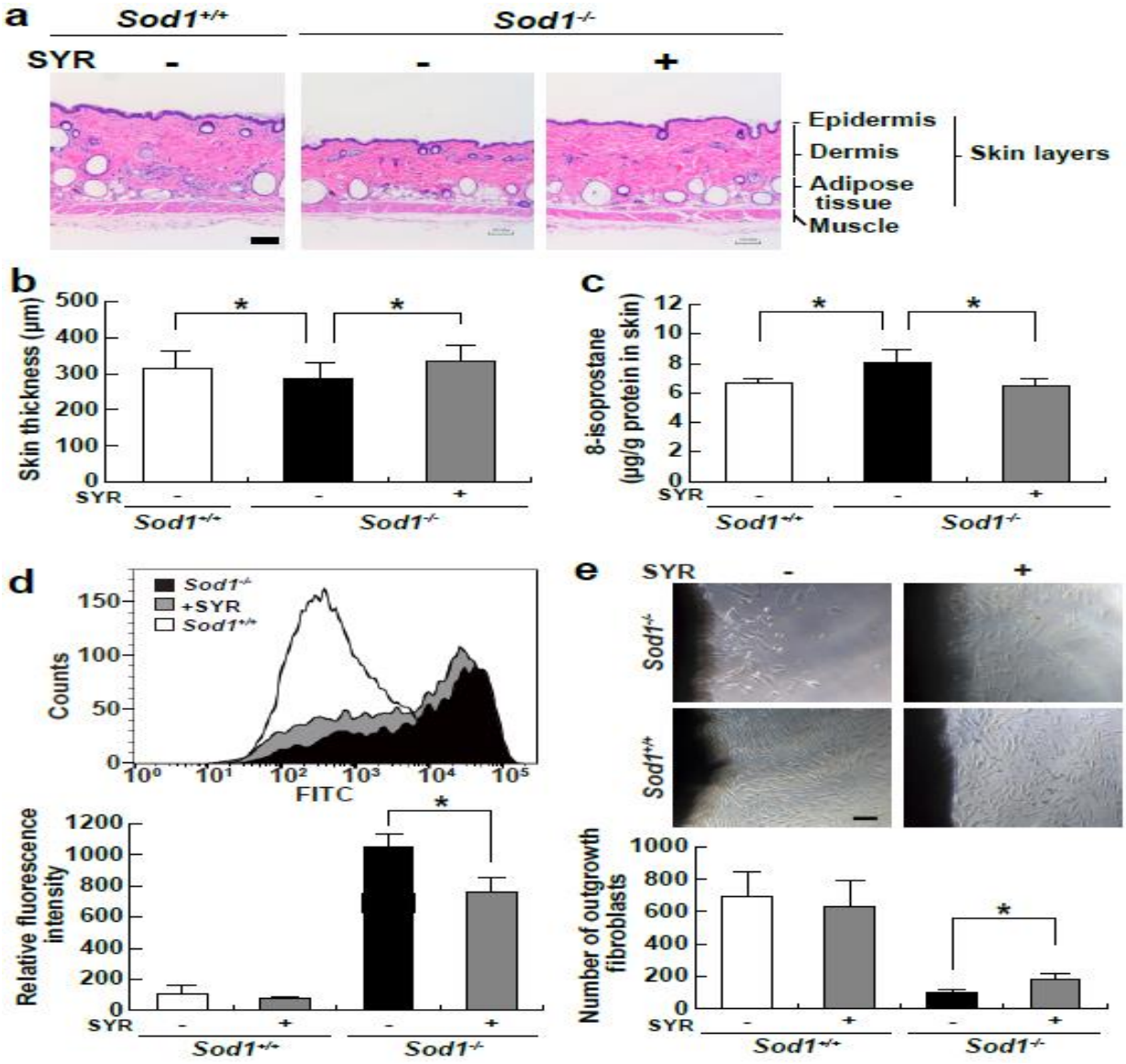

Figure 11. SYR attenuates skin atrophy and oxidative damage in *Sod1*$^{-/-}$ mice. (a) Hematoxylin and eosin staining of the back skin of *Sod1*$^{-/-}$ and *Sod1*$^{+/+}$ mice orally treated with SYR (50 mg/kg/day) for 8 weeks between 16 to 24 weeks of age. (b) The thicknesses of the total back skin layers of the knockout and wild-type mice orally treated with SYR (50 mg/kg/day) for 8 weeks from 16 to 24 weeks of age. (n = 9–10). (c) Absolute 8-isoprostane levels in the back skin of *Sod1*$^{-/-}$ and *Sod1*$^{+/+}$ mice orally treated with SYR (50 mg/kg/day) for 8 weeks between 16 to 24 weeks of age. (n = 9–10). (d) Relative intracellular ROS levels in primary *Sod1*$^{-/-}$ and *Sod1*$^{+/+}$ fibroblasts treated with 50 μM SYR for 72 h, as measured using 2',7'-dichlorodihydrofluorescein (DCF) (n = 3). (e) Number of outgrown fibroblasts in *Sod1*$^{-/-}$ and *Sod1*$^{+/+}$ skin disc cultures treated with 50 μM SYR for 72 h (n = 6–8). The statistical evaluations were performed using Dunnett's or Student's t-tests. Data represent the mean ± SD; $^{*}p < 0.05$. The scale bar represents 100 μm.

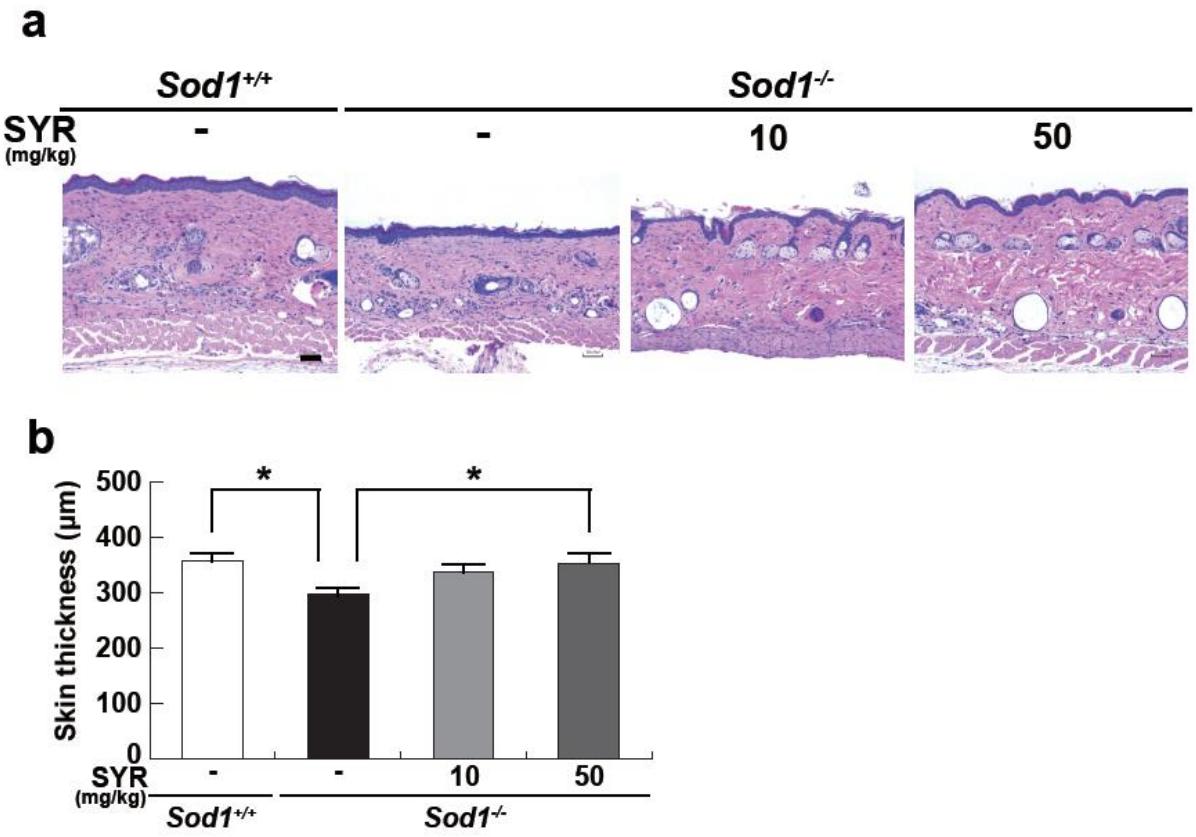

Figure 12. Effects of syringaresinol on skin atrophy. (a) Hematoxylin and eosin staining of the back skin of hairless *Sod1*$^{-/-}$ (knockout) and hairless *Sod1*$^{+/+}$ (wild type) mice orally treated with syringaresinol (SYR, 10 or 50 mg/kg/day) for 8 weeks between 6 to 14 weeks of age. (b) The thicknesses of the total back skin layers of *Sod1*$^{-/-}$ and *Sod1*$^{+/+}$ mice orally treated with SYR (10 or 50 mg/kg/day) for 8 weeks from 6 to 14 weeks of age. (n = 12–13). The statistical evaluations were performed using ANOVA Dunnett's test. Data represent the mean ± SD; *p < 0.05. The scale bar represents 100 μm.

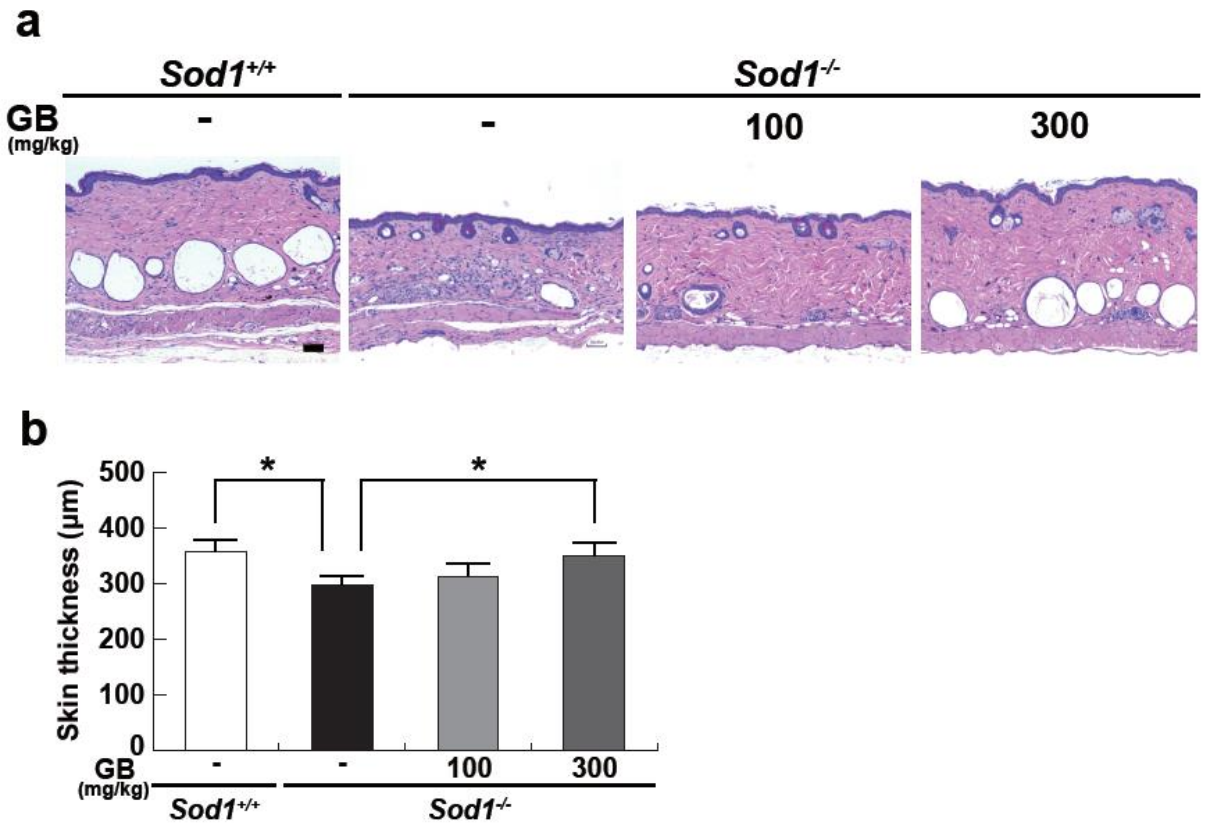

Figure 13. Effects of ginseng berry on skin atrophy and oxidative damage in SOD1 knockout mice. (a) Hematoxylin and eosin staining of the back skin of hairless *Sod1*$^{-/-}$ (knockout) and *Sod1*$^{+/+}$ (wild type) mice orally treated with the ginseng berry (GB, 100 or 300 mg/kg/day) for 8 weeks between 6 to 14 weeks of age. (b) The thickness of total skin area of the back skin of the *Sod1*$^{-/-}$ and *Sod1*$^{+/+}$ mice orally treated with GB (100 or 300 mg/kg/day) for 8 weeks from 6 to 14 weeks of age. (n = 12–13). The statistical evaluations were performed using ANOVA Dunnett's test. Data represent the mean ± SD; *p < 0.05. The scale bar represents 100 μm.

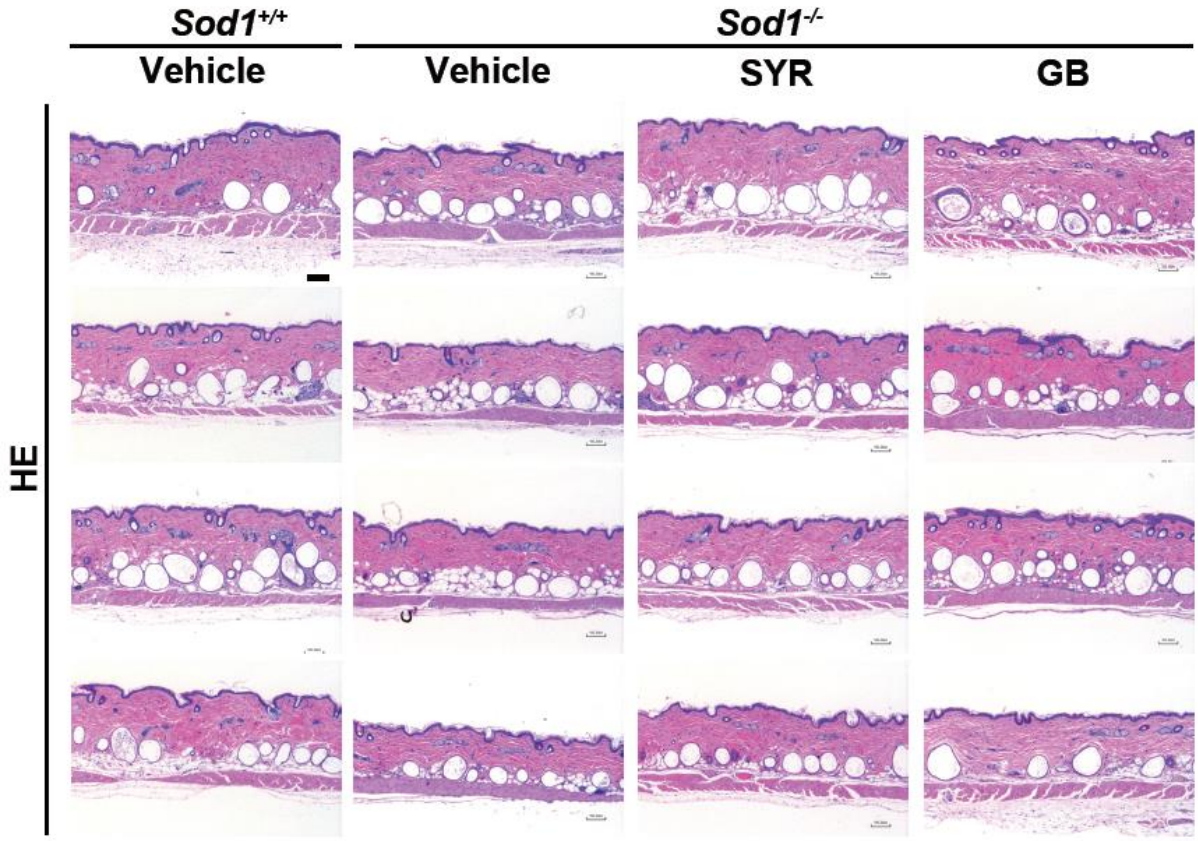

Figure 14. Effects of syringaresinol and ginseng berry on skin atrophy in SOD1 knockout mice. Hematoxylin and eosin staining of the back skin of hairless *Sod1*$^{-/-}$ (knockout) and *Sod1*$^{+/+}$ (wild type) mice orally treated with the SYR (50 mg/kg/day) or GB (300 mg/kg/day) for 8 weeks between 16 to 24 weeks of age (n = 4). The scale bar represents 100 μm.

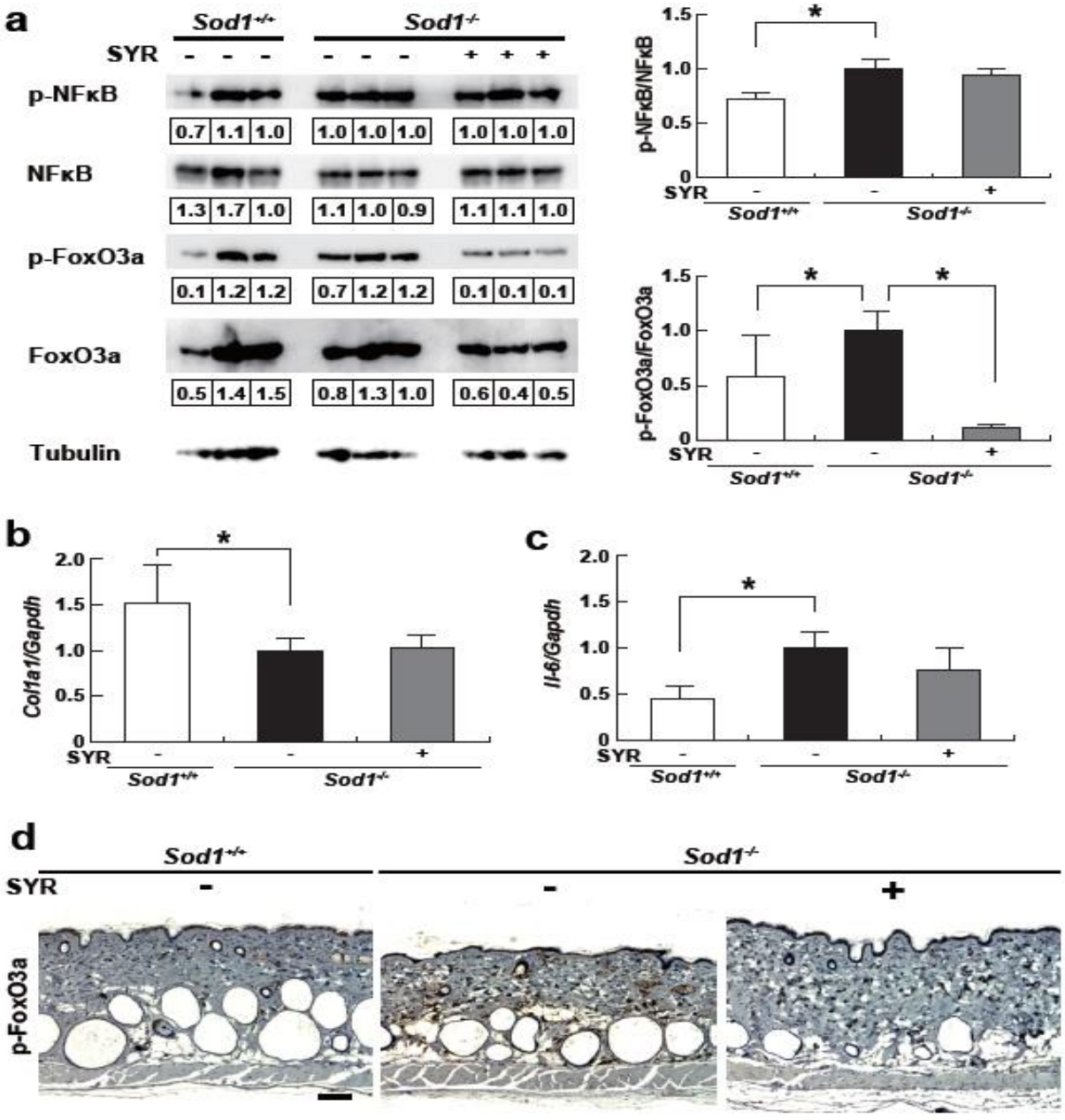

Figure 15. SYR decreases phosphorylation of FoxO3a, but not NF-κB, in *Sod1*$^{-/-}$ skin. (a) Western blotting of total NF-κB, phosphorylated NF-κB, total FoxO3a, and phosphorylated FoxO3a levels in the back skin of *Sod1*$^{-/-}$ and *Sod1*$^{+/+}$ mice orally treated with SYR (50 mg/kg/day) for 8 weeks between 16 to 24 weeks of age. Full blotting data presented in Supplematary Figure S7. The mRNA levels of the NF-κB downstream genes procollagen 1a1/*Col1a1* (b) and interleukin-6/*Il-6* (c) in the back skin of *Sod1*$^{-/-}$ and *Sod1*$^{+/+}$ mice orally treated with SYR (50 mg/kg/day) for 8 weeks between 16 to 24 weeks of age. The data were normalized to the housekeeping gene glyceraldehyde-3-phosphate dehydrogenase/*Gapdh* expression (n = 4 each group). (d) Immunohistochemical staining for phosphorylated FoxO3a was performed on the back skin sections prepared from *Sod1*$^{-/-}$ and *Sod1*$^{+/+}$ mice orally treated with SYR (50 mg/kg/day) for 8 weeks between 16 to 24 weeks of age. The statistical evaluations were performed using Student's *t*-test. Data represent the mean ± SD; $^{*}p < 0.05$. The scale bar represents 100 μm.

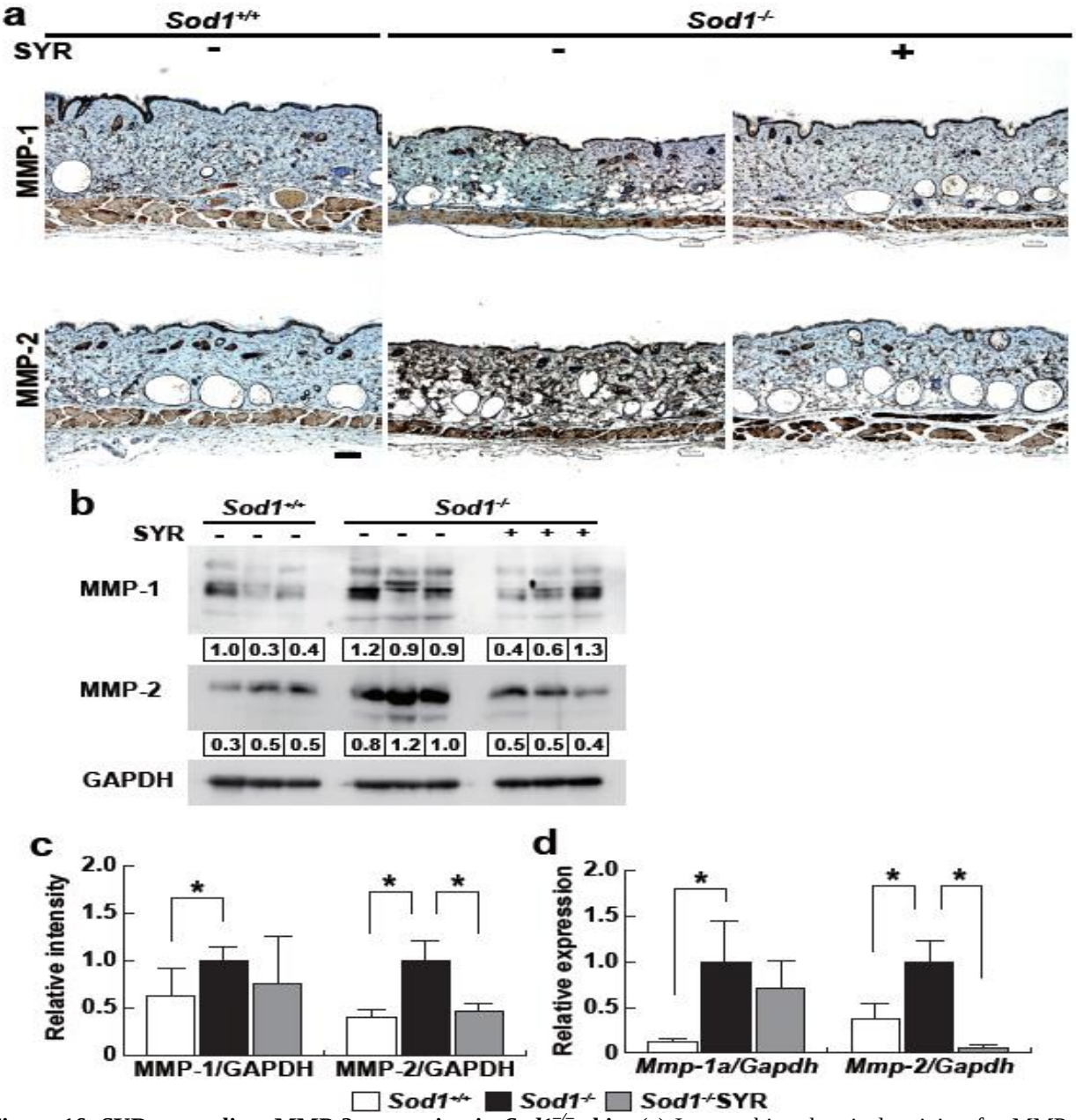

Figure 16. SYR normalizes MMP-2 expression in *Sod1*$^{-/-}$ skin. (a) Immunohistochemical staining for MMP-1 and MMP-2 in back skin sections prepared from *Sod1*$^{-/-}$ and *Sod1*$^{+/+}$ mice orally treated with SYR (50 mg/kg/day) for 8 weeks between 16 to 24 weeks of age. Western blotting bands (b) and graphic presentations (c) of MMP-1 and MMP-2 levels in the back skin of *Sod1*$^{-/-}$ and *Sod1*$^{+/+}$ mice orally treated with SYR (50 mg/kg/day) for 8 weeks between 16 to 24 weeks of age. Full blotting data presented in Supplementary Figure S7. (d) mRNA expressions of *Mmp-1a* and *Mmp-2* in the back skin of *Sod1*$^{-/-}$ and *Sod1*$^{+/+}$ mice orally treated with SYR (50 mg/kg/day) for 8 weeks between 16 to 24 weeks of age. The data were normalized to the housekeeping gene glyceraldehyde-3-phosphate dehydrogenase/*Gapdh* expression (n = 4 each group). The statistical evaluations were performed using Student's t-test. Data represent the mean ± SD; $^{*}p < 0.05$. The scale bar represents 100 μm.

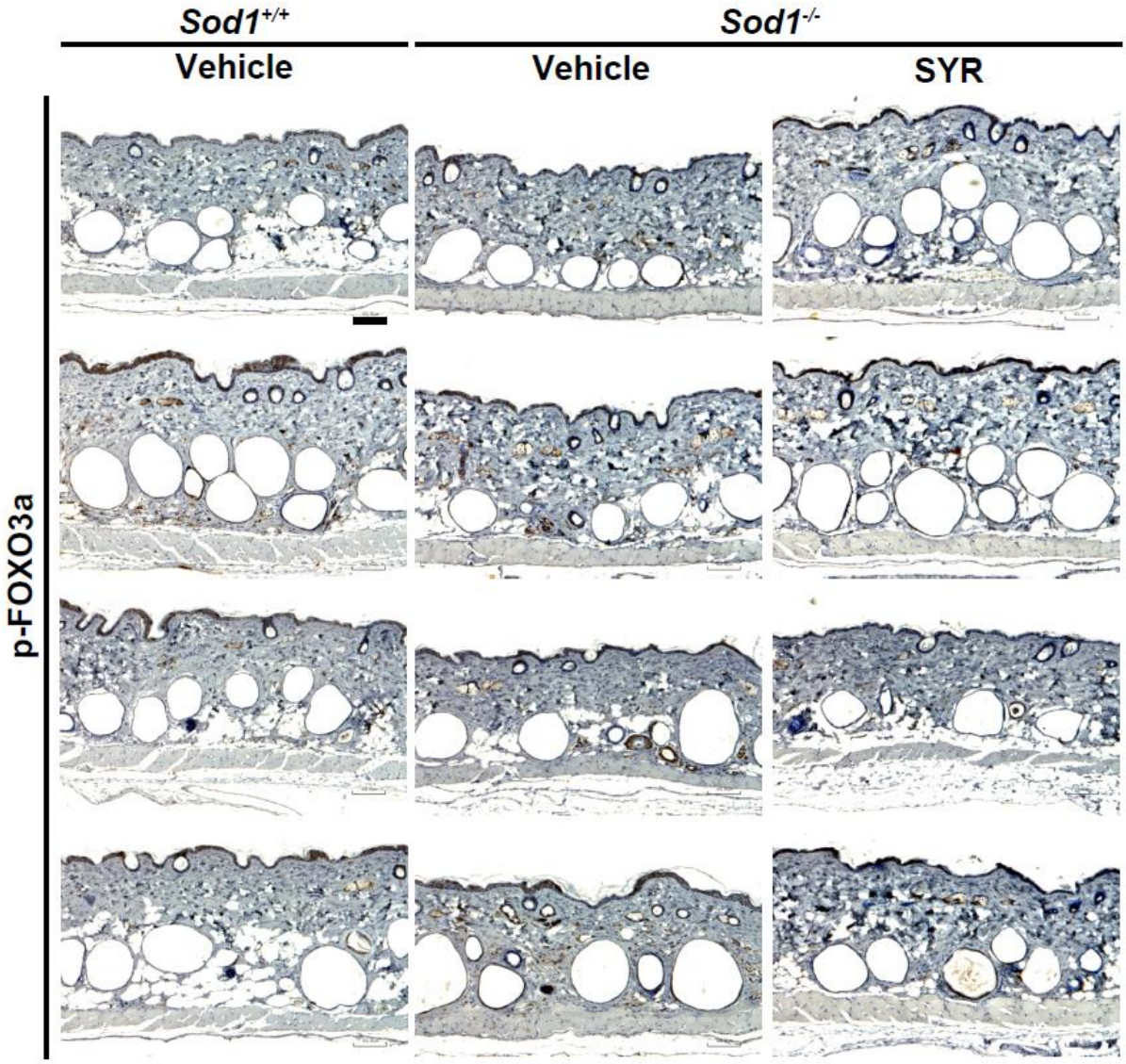

Figure 17. Syringaresinol treatment inhibits the phosphorylation of FoxO3a in mouse skin. The immunohistochemical staining of phosphorylated FoxO3a was subjected on the back skin sections prepared from *Sod1*$^{-/-}$ and *Sod1*$^{+/+}$ mice orally treated with the SYR (50 mg/kg/day) for 8 weeks between 16 to 24 weeks of age (n = 4). These sections were counterstained with hematoxylin. The scale bar represents 100 μm.

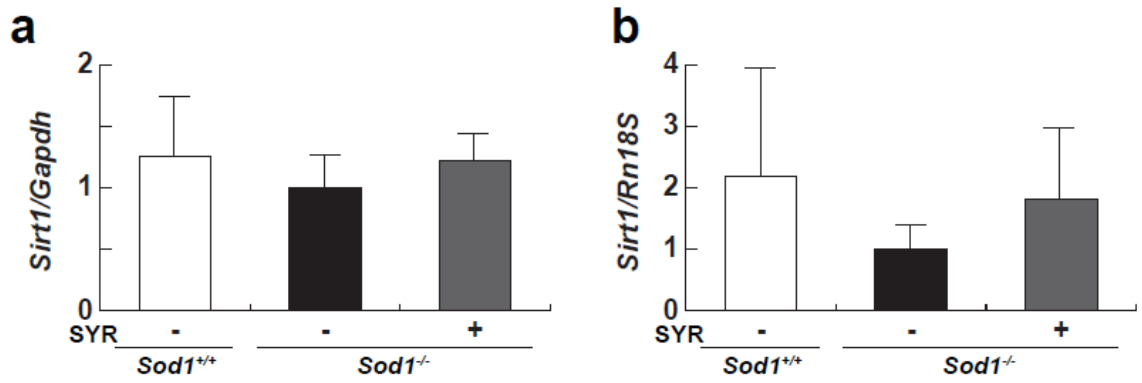

Figure 18. The expressions of *Sirt1/Gapdh* (a) and *Sirt1/Rn18S* (b) in the back skin of *Sod1*$^{-/-}$ and *Sod1*$^{+/+}$ mice orally treated with the SYR (50 mg/kg/day) for 8 weeks between 16 to 24 weeks of age. These data indicates that any significations were not observed.

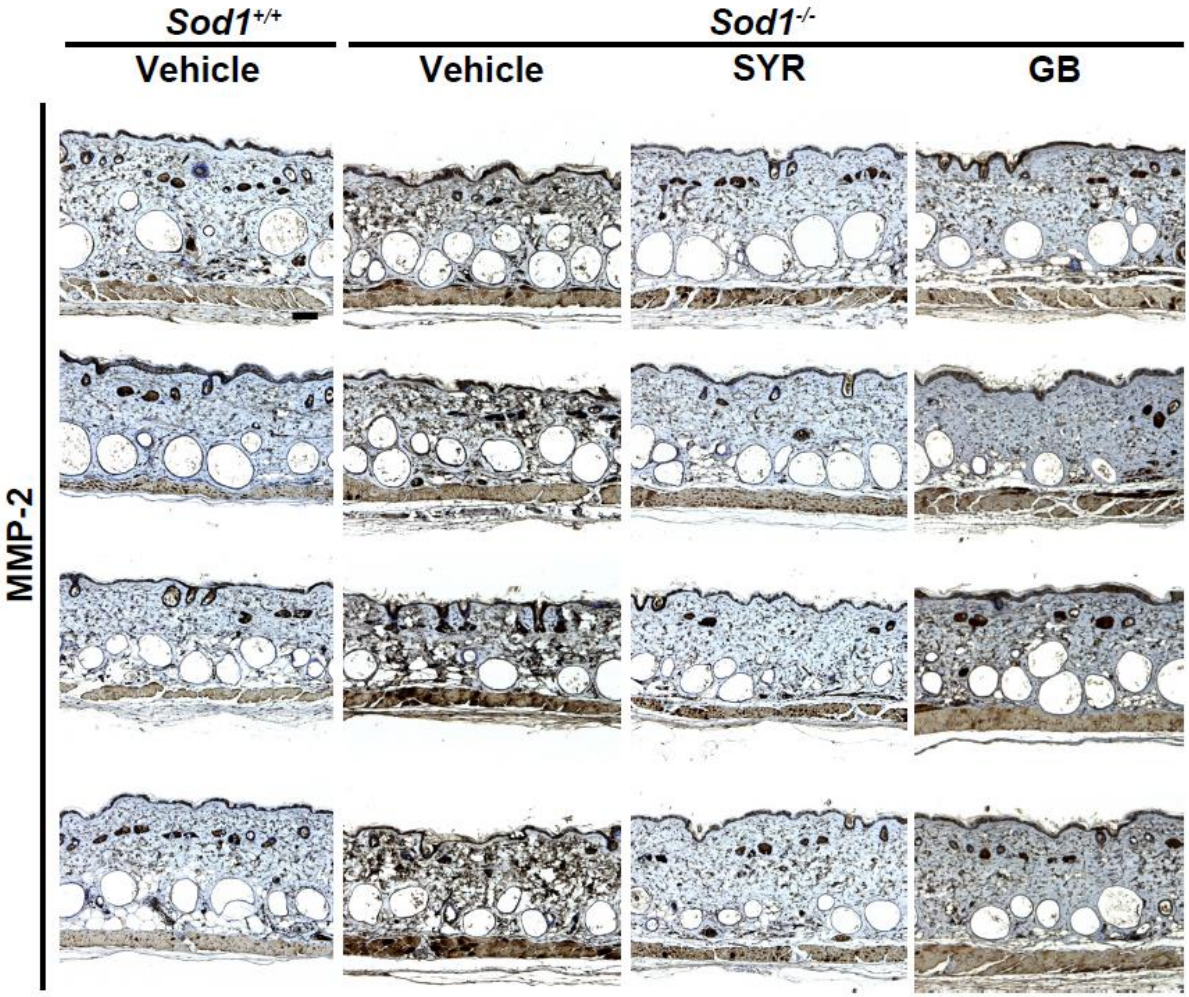

Figure 19. FoxO3a activation by syringaresinol associates with suppression of MMP-2 expression. The immunohistochemical staining of MMP-2 was subjected on the back skin sections prepared from *Sod1*$^{-/-}$ and *Sod1*$^{+/+}$ mice orally treated with the SYR (50 mg/kg/day) for 8 weeks between 16 to 24 weeks of age (n = 4). These sections were counterstained with hematoxylin. The scale bar represents 100 μm.

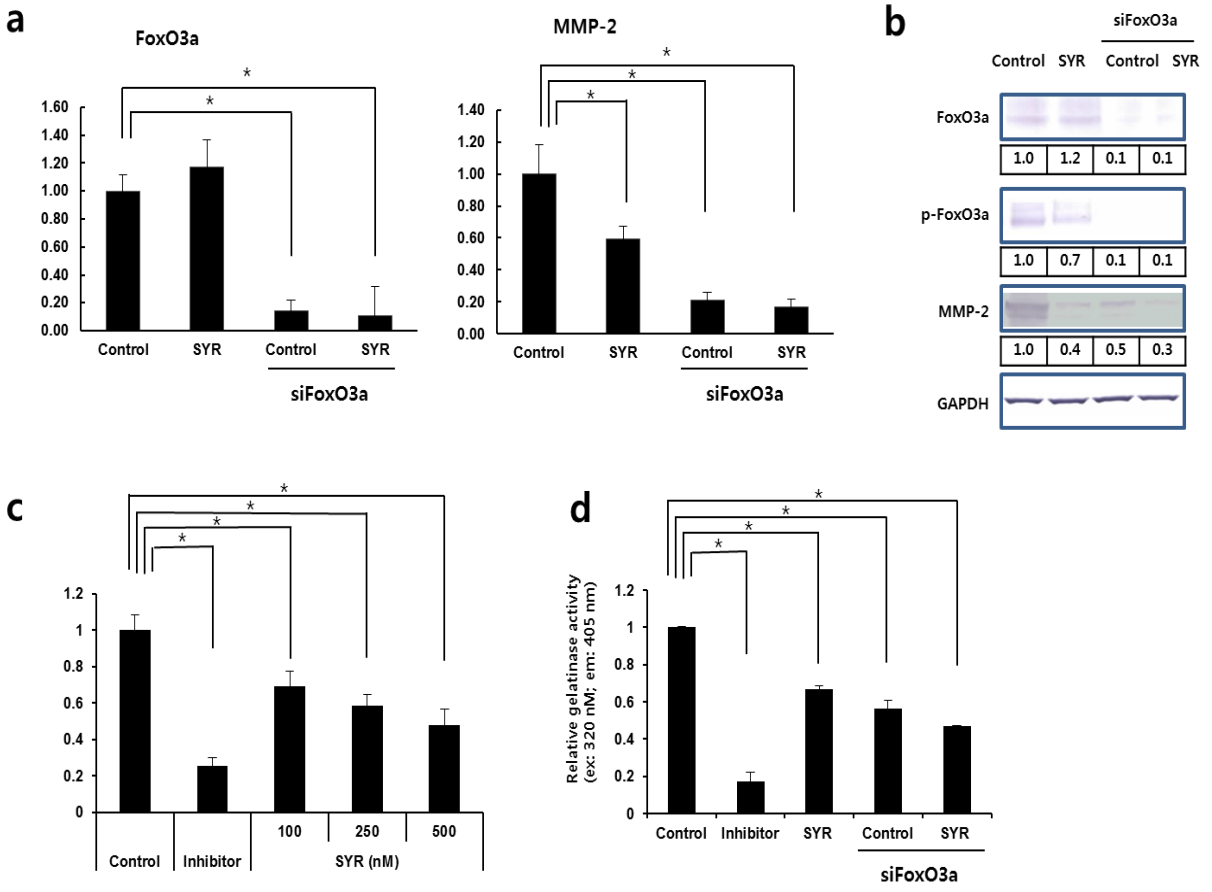

Figure 20. SYR lowered MMP-2 expression and also gelatinase activity in FoxO3a-dependent manner. Human dermal fibroblasts were transfected with small interfering RNAs (siRNAs) against FoxO3a for 48 hours. (a) The expressions of *foxo3a* and *mmp-2* genes were analyzed by means of quantitative real-time reverse transcriptase PCR (RT-qPCR). *$P < 0.05$. (b) After treatment with FoxO3a siRNAs and 500 nM SYR for 2 days, the cell lysates were analyzed by western blot analysis. (c-d) The MMP-2 gelatinase activity of cell lysates was measured by gelatinase fluorogenic assay kit at an excitation wavelength of 320 nm and an emission wavelength of 405 nm. *$P < 0.05$.

The Journal of Investigative Dermatology

平成31年 2月19日　印刷中

The Journal of Investigative Dermatology vol. 134 No. 5

平成26年１月２日　公表済